Analysis of Radiosonde and PWV data from the 2004 North Slope of Alaska Arctic Winter Radiometric Experiment

V. Mattioli[1], E. R. Westwater[2], D. Cimini[2], J. S. Liljegren[3], B. M. Lesht[3]
S. Gutman[4], and F. Schmidlin[5]
[1]Dipartimento di Ingegneria Elettronica e dell'Informazione, Università di Perugia via G. Duranti 93, 06125 Perugia, Italy
[2]Cooperative Institute for Research in Environmental Sciences, University of Colorado/NOAA-Environmental Technology Laboratory, 325 Broadway, Boulder, CO 80305, USA
[3]DOE/Argonne National Laboratory, Bldg 203, 9700 South Cass Avenue, Argonne, IL 60439, USA
[4] NOAA/Forecast Systems Laboratory, 325 Broadway, Boulder, CO 80305, USA
[5] NASA Wallops Flight Facility, Goddard Space Flight Centre, Wallops Island, Virginia, USA

Introduction

Many years of research and experiments conducted by investigators of the Atmospheric Radiation Program (ARM) have focused on radiosonde measurements of humidity, primarily because of their importance to modeling of radiative transfer [Clough, 1999]. Many of these experiments have been conducted in the mid-latitudes [Revercomb et al., 2003], or in the tropics [Westwater et al., 2003; Wang et al., 2002]. However, there is a dearth of radiosonde comparisons for Arctic locations. In March 1999, an Intensive Operating Period (IOP) was conducted at the ARM's "Great White" field site near Barrow, Alaska [Racette et al., 2005]. Due to a limited number of radiosondes, many questions were unanswered about the accuracy of radiometric remote sensors. To better understand these and other issues, a one-month period, the 2004 North Slope of Alaska Arctic Winter Radiometric Experiment was conducted from March 9 to April 9, 2004. In this experiment, we compared several radiosonde observations (RAOB) and remote sensing instruments measurements. A description of the experiment is given by Westwater et al., 2004, and initial results are also contained in these proceedings [Cimini et al., 2005; Westwater et al., 2005]. The focus in this paper is on the comparisons of radiosonde measurements of temperature and relative humidity profiles, as well as the comparison of measurements of precipitable water vapor (PWV) by radiosondes, the Microwave Radiometer (MWR), the Microwave Profiler (MWRP), and a Global Positioning System (GPS) receiver.

Analysis of Radiosondes

During the 1999 IOP, daily Vaisala RS80 radiosondes were launched at the Great White and the synoptic radiosondes from the National Weather Service (NWS) were also available. In 2004, many simultaneous and nearly co-located launches of radiosondes allowed us to compare various aspects of temperature and humidity measurements that

are of immediate relevance to ARM. In particular, we present the analysis of radiosonde soundings from three different humidity sensors that were launched from three separate locations near Barrow. ARM Operational Balloon Borne Sounding System (BBSS) radiosondes were launched daily at 2300 UTC at the Great White. These BBSS sondes used Vaisala RS90 humidity elements. In addition, at the ARM Duplex, 2.2 km to the west of the Great White, BBSS radiosondes were launched four-times daily (500, 1100, 1700, and 2300 UTC). Raw data from synoptic radiosondes from the NWS (1100 and 2300 UTC) were also archived. The NWS site is 4.3 km to the southwest of the Great White. Finally, during clear conditions, eight dual-radiosonde launches were operated by NASA at the ARM Duplex. Table 1 shows the location of the three RAOB sites.

Radiosonde types

VAISALA RS90 at the ARM Duplex and the Great White

From the beginning of the experiment, radiosondes of Vaisala RS90-A type were launched at the ARM Duplex (DPLX) in Barrow and at the ARM Great White (GW) site. For convenience, these radiosondes will be referred to as DPLX-RS90 and GW-RS90, respectively.
The RS90-A is a "PTU-only" system, i.e., the primary measurements are pressure, temperature (T), and relative humidity (RH). Altitude and dew point temperature are derived quantities in the data. The sensor for the temperature measurement is the Vaisala F-Thermocap, which consists of a capacitive wire. The sensor for the relative humidity is the Vaisala H-Humicap, a thin film capacitor with a heated twin-sensor design: two humidity sensors work in phase so that while one sensor is measuring, the other is heated to prevent ice formation [www.vaisala.com]. Samples were taken every 2 seconds. Details of the sensors are also given in Paukkunen et al., 2001.

NWS VIZ-B2 at Barrow

During the experiment, the synoptic radiosondes launched in Barrow by the U.S. National Oceanic and Atmospheric Administration /NWS were also collected. These radiosondes are Sippican VIZ-B2 type. The VIZ radiosondes were used at all NWS stations until 1995, when NWS started a process of replacement with radiosondes manufactured by Vaisala. The VIZ-B2 measure pressure, temperature, relative humidity, wind direction and wind speed every 6 seconds. Altitude and dew point temperature are derived quantities in the data. These soundings are also operationally sampled and made available by the NOAA/Forecast System Laboratory (FSL) [http://raob.fsl.noaa.gov]. Here, these soundings will be referred to as NWS-VIZ. The sensor for the temperature measurement is a rod thermistor, and the sensor for humidity measurements is a carbon hygristor (CH), whose characteristics are described in NWS, 1999.

Snow White at the ARM Duplex

During the experiment, eight successful dual radiosondes were released by NASA at the ARM Duplex, three during the day and five during the night. Two radiosonde packages were attached to the same balloon. The first package was the ARM BBSS. The second

package was a radiosonde of Sippican GPS Mark II type that was modified to contain a Snow White chilled mirror dew-point hygrometer (SW-CM). This instrument is manufactured by Meteolabor AG, Switzerland [http://www.meteolabor.ch], and is a dew-point sensor designed for radiosonde application. The performance of the chilled mirror hygrometer has been evaluated in many studies [Fujiwara et al., 2003; Voemel et al., 2003; Wang et al., 2003]. In addition to the chilled mirror sensor, the package also contained a VIZ carbon hygristor humidity sensor. For convenience, we will refer to the latter sensor as SW-CH.
A GPS receiver and antenna were included in the system and integrated into the radiosonde electronics [www.sippican.com]. Wind data and pressure values (by applying the hydrostatic equation with the GPS altitude) are derived from the GPS data processing, so that a pressure sensor was not included. The system used a thin rod thermistor for temperature measurements. Samples were taken every 1.2 seconds. Dew point temperature is computed from the CH measurements. Three spare channels were also included in the system, and used to transmit the data from the attached SW-CM.

Radiosonde data processing

After a series of quality control procedures were taken, some data were eliminated. Table 2 shows the available soundings after initial quality control. In addition, soundings were filtered because of the presence of spikes in the humidity measurements (see section on RAOB filtering). Finally, for purposes of statistical comparisons, the soundings were fitted to a regular grid by applying a linear interpolation over height, with the following specifications:

- a resolution of 10m up to 10 km;
- resolution of 100 m from 10 km to the highest level.

These general specifications yield height steps for each set of sondes as follows:
DPLX-RS90 sondes: H (m) = 8 (surface), 14, 20, 30, 40…10000, 10100…..
GW-RS90 sondes: H (m) = 8 (surface), 14, 20, 30, 40…10000, 10100…..
NWS-VIZ sondes: H (m) = 12 (surface), 20, 30, 40…10000, 10100…..
SW sondes: H (m) = 10 (surface), 20, 30, 40…10000, 10100…..
These interpolated and quality-controlled data are called Level 2.0 and were used for the subsequent comparisons of the temperature and humidity profiles.
After the intercomparison between the radiosoundings, and with remote sensing instruments (GPS, MWR, MWRP), some outliers have also been identified. Their number for each radiosonde type is given in the parentheses in Table 2.

RAOB filtering

In processing the RAOB, we identified spurious data in the relative humidity data in approximately 50% of the DPLX-RS90 soundings, and to lesser extent, in some of the GW-RS90 soundings.
Since the dew-point temperature is a derived quantity in the data, it is also affected by this noise. Temperature measurements were not affected by this problem. The spurious

data were manifested generally above 10 km from the surface; the origin of the problem is still under investigation, but seems to be associated with the switching between the two humidity elements on the RS90. Figure 1 shows the noisy RH and dew point temperature measurements in a DPLX-RS90 sounding. In general, it is possible to recognize the behavior of the true profile behind the spikes by continuity assumptions. Following these considerations, we applied a non-linear filter to detect and replace these high-frequency interferences in the data. Noisy points were identified by using a median high-pass filter, and then corrected by interpolation over the adjacent points. The window of the filter varied with the noise magnitude and hence varied from radiosonde to radiosonde. Figure 1 also shows the reconstructed profiles. The filter works properly when the interferences are infrequent, and it is possible to estimate the missing value from contiguous points not affected by the noise. Because of the extent of the spurious data, a wide window of the filter (> 60-point window) was applied to 35 radiosoundings. For four of them, in particular for the soundings launched on March 26 at 500 UTC, the extent of the spurious data did not allow a complete reconstruction of such profiles, which are eventually affected by some spurious data.

Comparison of RAOB temperature and relative humidity measurements

In this section, a statistical evaluation of the temperature and relative humidity measured by the different sensors is presented. Figure 2 shows the sounding profiles taken on March 26 at 2300 UTC, from the various radiosonde types. Particular attention is given to the dual launches. As mentioned above, dual launches provide unique opportunities to compare different radiosonde types, since the difference in the measurement is only due to the sensor type and not to temporal or spatial displacements.

GW-RS90 vs. DPLX-RS90 profiles

Figure 3 shows the temperature and relative humidity difference profiles between the DPLX-RS90 and the GW-RS90 soundings. The average difference profile (red line) and standard deviation (std) profile (orange line) are also given. The difference of the RAOB profiles is performed level by level by using the Level 2.0 data, in which the measurements were interpolated on the same vertical grid. Small differences are present in the difference profiles, which can be attributed to the spatial baseline (2–3 km) and temporal baselines (less than 15 min) between the launches at the DPLX and at the GW. In Figure 3 we note a temperature bias near the surface (DPLX warmer than GW) of about 0.8 °C, which decreases up to some 100 m. Above 100 m, the temperature difference stays within 0.3 °C, with an average rms value of 0.26 °C. For the RH, the mean difference stays within 2%, with average rms value of 2.5%.
The anomalous std values around 12–14 km and at 20 km in the RH difference profile of Figure 3 (orange line) are due to some spurious noise that still affects the RH measurement of the DPLX-RS90.

NWS-VIZ vs. DPLX-RS90 profiles

Figure 4 shows the temperature difference profiles between the VIZ-B2 soundings operated by the NWS and the Vaisala RS90 soundings launched at the DPLX.
Two features can be noticed. First, there is a gradient in temperature around 100–300 m (with the temperature over the NWS station higher than over the DPLX). The gradient in temperature is also present in the temperature comparison of NWS-VIZ radiosondes and the GW-RS90 (not shown). This phenomenon could be explained by the presence of local heating in the town of Barrow. In fact, the NWS station is in the town, the DPLX is located in the periphery of the town, and GW is the farthest site from the town.
Second, above 10 km the std of the difference increases with height. The average rms of the temperature difference is 0.6 °C, but it is 0.42 °C below 10 km and 1.7 °C above it.
Figure 5 shows the temperature comparison when the dataset is divided into data taken at night at 1100 UTC (2 a.m. local time) and during the day at 2300 UTC (2 p.m. local time). This partition indicates that the std difference profile above 10 km of Figure 4 is a consequence of a bias (up to -5 °C) between the NWS temperature and the DPLX, negative during the night and slightly positive during the day. This behavior is also confirmed in the comparison with the GW-RS90. Although the Vaisala and the NWS-VIZ radiosondes use different types of temperature sensors, it is not clear why the two radiosondes basically agree during the day, but have substantial differences at night.
Figure 6 (a) shows statistical comparisons of the RH measurements. In the first 300 m, the RH profiles of NWS-VIZ radiosondes are 5% lower on average with respect to the DPLX-RS90. Above this level, RH from the NWS-VIZ carbon hygristor is in mean larger than the one from Vaisala H-Humicap at the DPLX. This bias increases to about 20%, starting at approximately 8 km. The average RH difference is 4% below 10 km, but increases to 16% above 10 km (above the troposphere). The average rms difference below and above 10 km is 12% and 18%, respectively. In one occasion, the bias reached values as high as 40%. This sounding, taken on April 9 at 2300 UTC, is shown in Figure 6 (b).
There are some significant negative excursions that occur in the point-by-point comparisons. One example is shown in Figure 6 (c) in which there is a -70% value of the RH difference between 5 and 6 km in the soundings taken on March 21 at 2300 UTC. Here the RH from the carbon hygristor reached values as low as 1%. The -60% value of the RH difference at about 4 km in Figure 6 (a) occurred on March 22 at 11 UTC. These particular examples are discussed again in section “Intercomparison of PWV measurements.”

Comparison with the Snow White radiosondes

Figure 7 shows the difference between the humidity profiles taken by the NWS-VIZ radiosondes and the NASA SW-CM and SW-CH sensors. Figure 7(a) gives the comparison between two humidity sensors of the same type (the VIZ CH). Figure 7(b) gives the comparison between the NWS-VIZ CH and the SW-CM. Figure 7(c) shows the comparison between the two different sensors, SW-CH and SW-CM, mounted on the package launched by NASA.
As is expected, the comparison shows good agreement between the measurements of the two carbon hygristors. The only exception was for the NWS-VIZ sounding taken on

March 18, at 1100 UTC. On that occasion, the RH profile from the NWS-VIZ resembles the RH profile from the SW-CH, but was consistently lower than the other soundings (Figure 7(d)).
On the other hand, the CH measurements (both SW-CH and NWS-VIZ) show a significant bias with respect to the SW-CM above 8–10 km (generally, above the tropopause), as evident in Figure 7(b-c). In particular, the average RH difference between the carbon hygristor and the chilled mirror mounted on the same radiosonde operated by NASA is 7% below 8 km, while 26% above 10 km. Similarly, the average RH difference between the NWS-VIZ and the SW-CM is 6% below 8 km, and 20% above 10 km. This is consistent with the results obtained using the DPLX-RS90 instead of SW-CM radiosondes (Figure 8(left)).
Finally, the dual-launch comparison between RH profiles obtained by the SW-CM and the Vaisala H-Humicap shows a much better agreement, with an average value of -0.5%, and an average rms difference on the order of 5%, as shown in Figure 8 (right).

PWV comparison among radiosonde types

In addition to the level-by-level comparison, in this section we compare the radiosonde types in terms of PWV. Figure 9 shows the PWV time series computed from the various radiosondes. Some features can be noticed.
- NWS-VIZ sondes provide in general high values of PWV with respect to the Vaisala RS90 (launched at both DPLX and GW).
-The PWV from the SW-CM agrees very well with data from the Vaisala radiosondes, while the PWV computed from the SW-CH is usually larger than the ones computed from both the Vaisala and the SW-CM.
-Moreover, PWV computed from the SW-CH data are closer to the values obtained from the NWS-VIZ radiosondes.
These considerations are in agreement with the difference observed in the carbon hygristor humidity profiles with respect to the Snow White chilled mirror and the Vaisala H-Humicap measurements.
In Figures 10–14, the statistical analysis is shown in scatterplots; the values of bias, std, slope and intercept of a linear fit are also listed. The number of available SW radiosondes is not sufficient for a significant statistical comparison, but the analysis can give a useful indication of the general behavior.
As can be noticed from Figure 10 (left), the presence of three outliers affects the slope of the regression line in the comparison of the NWS-VIZ with the DPLX-RS90 radiosondes, as well as the bias (NWS-DPLX), while the PWV from the NWS-VIZ radiosondes is generally higher than the PWV from the DPLX-RS90 radiosondes.
The two PWV low values from the NWS-VIZ with respect the DPLX-RS90 (around 0.96 and 1.13 cm, respectively) are derived from NWS soundings taken on March 21, at 2300 UTC and on March 22, at 1100 UTC (see comments on Figure 6 (a), and Figure 6 (c)). The higher value (0.78 vs. 0.57, respectively) is derived from NWS soundings taken on April 9, at 2300 UTC (see Figure 6 (b)). Such cases have been also investigated using remote sounding data (see also Figure 18 in section “PWV comparisons between MWR MWRP, GPS and the radiosondes”).
Removing these values in the statistics gives the results shown in Figure 10 (right): the values of the bias and the slope are consistent with the comparison with the other

instruments. The outliers, shown in the scatterplot, are enclosed in red circles. A forth outlier (around 0.1 cm), was also removed from the statistics. It corresponds to the sounding taken on March 18 at 11 UTC (see also Figure 7 (d)). Such outliers were also removed in the statistics of Figure 11 and Figure 12 (c)).
The comparison of PWV from SW-CH shows a consistent bias (on the order of 0.03 cm) with respect to the PWV from the other sensor types, and except for the apparently erroneous sounding of March 18, at 1100 UTC it is closer to PWV from NWS.
Figure 13 (left) shows the comparisons of PWV from the DPLX-RS90 and the GW-RS90, and Figure 13 (right) gives the comparison of PWV from the DPLX-RS90 and the SW-CM for the dual launches. Good agreement can be noticed, between the PWV from the SW-CM and the Vaisala, with a rms difference of the order of 0.008 cm.
The rms difference between the PWV values from the GW-RS90 and the DPLX-RS90 is 0.011 cm, and the rms difference between NWS-VIZ and SW-CH sensor is 0.013 cm. These differences include diversities due to both to the spatial baseline and sensor accuracy.
The rms difference between PWV from the GW-RS90 and from the NWS-VIZ is 0.071 cm, and between the DPLX-RS90 and the NWS-VIZ is 0.062 cm. The higher bias for the NWS-VIZ in the comparison with the GW-RS90 data can be explained by taking into account that the comparison involved only daytime soundings. When the comparison between NWS-VIZ and DPLX-RS90 involved data taken at 23 UTC, simultaneously with the GW launches, the bias (NWS-DPLX) was 0.058 cm. The rms difference between PWV data from NWS-VIZ and SW-CM sensor is 0.039 cm.

PWV comparisons between MWR, MWRP, GPS and the radiosondes

In this section, we summarize the comparisons of PWV obtained from the MWR and the MWRP operating at the Great White field site, with the PWV from a GPS receiver and from the radiosondes.

MWR

The MWR that operates at the Great White is a dual-channel water vapor radiometer of the WVR-1100 series from Radiometrics [www.radiometrics.com], operating at 23.8 and 31.4 GHz. The MWR scans at five elevation angles (19.35, 23.4, 30.15, 41.85 and 90.0 degrees) in the east–west direction. Two different tipping calibration algorithms were applied, the instantaneous tipcal calibration method (Han and Westwater, 2000) developed at the NOAA/Environmental Technology Laboratory (ETL) and the ARM calibration algorithm (Liljegren, 2000). Figure 14 shows a comparison of the PWV derived from MWR data that were processed by the two algorithms. Statistical comparisons are given later in this section.

MWRP

The MWRP is a twelve-channel radiometer of the TP/WVP-3000 series from Radiometrics, with five K-band channels (22.235, 23.035, 23.835, 26.235, and 30.0 GHz) and seven V-band channels (51.25, 52.28, 53.85, 54.94, 56.66, 57.29, and 58.8 GHz), which provide humidity and temperature profiles. The system includes also an infrared

broad-band radiometer and PTU sensors for the measurements of cloud base temperature and surface pressure, temperature, and humidity, respectively.
PWV can be retrieved from MWRP observations by using different combinations of channels (Liljegren and Lesht, 2004). For example, in this study we compare results obtained using only 2 channels, 23.835 and 30 GHz (2ch), the five K-band channels (5ch), and 6 channels, which are the five K-band plus the 51.25 GHz channel (6ch).

Both the MWRP and the MWR are provided with a wet window sensor that turns a heater on during condensing or precipitating conditions to promote the evaporation of rain or snow. In our comparisons, PWV data from the radiometers are accepted when the wet window sensor mounted on the radiometer indicated that the heater was not activated. However, as we show later in this section, in terms of PWV, the retrievals obtained when the heater is activated seem consistent with the observation s from other instruments (GPS, RAOBS).

GPS (Near real-time and Reprocessed)

A SuomiNet (http://www.suominet.ucar.edu) GPS receiver (SG27) located near the Great White provided PWV measurements throughout the experiment. The reliability of this site is generally very high, and it has been incorporated into the NOAA Forecast Systems Laboratory (FSL) ground-based GPS Meteorology network (http://gpsmet.noaa.gov). FSL and Scripps Institution of Oceanography collaborated to produce the near real-time (NRT) and reprocessed data used in this experiment.
Dual frequency carrier phase and surface meteorological observations were retrieved from this site in NRT and processed using the method described in Gutman et al., 2004a. In all manifestations of GPS data processing, the excess path length (or signal delay) of the GPS radio signal caused by the refractivity of the lower atmosphere, primarily the troposphere, is estimated as a free parameter in the calculation of the antenna position. As a rule, FSL imposes minimal constraints on this process to arrive at an independent and statistically robust solution that minimizes temporal observation error correlations. PWV is retrieved from the tropospheric signal delay by first parsing it into its wet and dry components by subtracting a hydrostatic delay calculated from surface pressure (Saastamoinen, 1972), and then mapping the wet component into PWV using a transfer function that is nearly proportional to surface temperature (Bevis et al., 1994).
The accuracy with which this can be accomplished in NRT (currently defined as less than 30-min latency) has been estimated by making long-term comparisons between GPS, MWR, and radiosonde PWV measurements, primarily at the SGP site near Lamont, OK. The results range from about 1.5 mm rms during the warm months with significant diurnal variations, to less then 0.75 mm rms during the cold months with negligible diurnal variations (Gutman et al., in preparation). Because of the time constraints imposed on data availability from operational weather forecasting, no special effort is made to reduce the impact of various sources of processing errors that are commonly contributed by factors described in Gutman et al., 2004b. These sources manifest themselves as noise or scatter about the mean in the NRT solution. Since the precision with which PWV is being measured in this experiment is virtually unprecedented, the normal variability of the GPS NRT measurement can be justifiably referred to as substantial compared to the MWR's.

An attempt to minimize the scatter was made by (1) implementing the post fit residual option in the GAMIT data software package (King and Boch, 1996) used by FSL, (2) using IGS precise orbits (rather than real-time hourly orbits provided to FSL by Scripps), and (3) identifying and removing non-random or repetitive aspects of the tropospheric delay time series that are probably associated with site-dependent multipath. Figure 15 shows the PWV time series of the NRT and the reprocessed data. The reprocessing step reduced most, but not all of the scatter in the GPS data, as can be noticed from Figure 16, which shows in detail the time series for March 9-20, 2004 and April 4-9, 2004, in which the excess noise in the GPS data is apparent with respect to the other instruments. In the following comparisons, only reprocessed GPS data will be used.

Intercomparison of PWV measurements

Figure 17 shows the PWV time series from the MWRP, retrieved by using six channels, the MWR (ARM calibration), the radiosondes launched at DPLX and the reprocessed GPS data. In general, there is good qualitative agreement between the measurements except at times when the GPS differs from the other sensors by about 1.5 mm. However, one of the strengths of GPS (i. e; the continuity of data during all weather conditions) is noted between days 80 and 82, when the wet rain flags eliminated radiometer data.
The simultaneous presence of the MWR, the MWRP and the GPS allowed us to further investigate the peculiar NWS-VIZ soundings identified in the radiosonde analysis, (see also Figures 6 (b-c) and Figure 10), that occurred on March 21 at 2300 UTC (Julian Day 81.958), on March 22 at 1100 UTC (Julian Day 82.460) and on April 9 at 23 UTC (Julian Day 100.959). In the comparison with the MWR, the MWRP and the GPS, we also found an outlier in the DPLX-RS90 radiosondes that occurred during March 22 at 1700 UTC. These cases are shown in Figure 18. Even though in some occasions the wet window flags were on, the data are of sufficient quality that the three RAOB outliers are easily recognized, and hence, have not been considered in the following statistical comparisons.
The statistical and scatterplot analyses of the comparisons between the GPS, the MWR and the various radiosonde types are shown in Figure 19 and Figure 20. The values of bias, std, slope and intercept of the linear fit are shown. As is seen, both the PWV from GPS and the MWR are greater than the DPLX-RS90 radiosondes by about 0.03-0.04 cm and less that the NWS-VIZ by about 0.015 cm. These results are consistent with the radiosondes comparisons shown previously in Figures 10-13, which show that the NWS-VIZ is greater than the DPLX-RS90 by about 0.05 cm. As for the PWV comparison among radiosonde types, the high bias in the GW data is explained by taking into account that the comparison involved soundings operated only during the day at 23 UTC. For daytime soundings, the bias in the comparison with the MWR is 0.045 cm for the DPLX-RS90 and -0.02 cm for the NWS-VIZ, respectively. Moreover, the DPLX-RS90 and the GW-RS90 differ by about 0.005 cm (see Figure 13 (left)).
Figure 21 is a scatterplot showing the comparison between the PWV from the MWR and the GPS, performed using 30-minute-averaged MWR data centered on GPS time.
The comparison shows a generally good agreement between the MWR and the GPS. The bias is negligible, and the std is on the order of 0.05 cm. Still, the fluctuations of the GPS data are apparent in the comparison with the MWR and the radiosondes. At the very low values the PWV from GPS have values as low as 0.07 cm, a value never reached by

MWR retrievals. In addition, at the very low PWV values, less than about 0.2 cm, the two calibrations for the MWR produce different results, and there could be sensitivity limits in the MWR retrieval algorithm at these low values. These discrepancies with the MWR should be further investigated, in particular in evaluating the retrieval coefficients from different models. Moreover, the use of higher frequencies, as for example the 183 GHz, should be investigated.
The rms difference of the PWV from RAOBs compared with PWV from the MWR and the GPS are summarized in Table 3. The rms values are generally good in terms of PWV, but at the low end of the range of PWV, less than 0.2 cm, the percentage differences are substantial, and approach 50%.

PWV from MWRP

The PWV from MWRP is retrieved by using measurements at 2 channels, 23.835 and 30 GHz (2ch), at 5 channels, 22.235–30 GHz (5ch), and at 6 channels, 22.235–30 and the 51.25 GHz (6ch). The PWV time series from these retrievals are shown in Figure 22. Monthly retrieval coefficients have been specifically computed from past radiosoundings using Vaisala radiosondes (RS80-H and RS90) launched from NSA-Barrow between 1998 and 2004, assuming a 0.3K rms error. All are based on the modified Rosenkranz model (Hitran width at 22 GHz, CKD 2.4 continuum; see Liljegren et al., 2005).
The 2-channel retrieval shows the larger scatter in the PWV, with values that reach zero. This behavior, compared to the 2-channel retrieval from the MWR is apparently due to the less frequent sampling of each channel of the MWRP with respect to the MWR. The use of 5 and 6 channels reduces this scatter considerably.
Figure 23 shows the time series of the PWV from the MWRP from the 6-channel retrieval and from the MWR, the analysis presented for both ARM and ETL calibration procedures.
Figure 24 shows the comparison of the PWV from the MWRP (from the three set of channels) with the PWV retrieved from the MWR in terms of scatterplots.
The retrievals from 5 and 6 channels agree better with the MWR than those from only the two channels, with a slightly better agreement of the 6-channel with the MWR, reducing the std by about 50%. The differences between ETL and ARM calibration are about 15% in rms. Figures 25-27 show the comparison of the PWV from the MWRP, retrieved by using 2, 5 and 6 channels, with the PWV from the radiosondes, respectively with the DPLX-RS90, the GW-RS90 and the NWS-VIZ. In Figure 28 the comparison with the GPS is given. PWV statistics in terms of rms are given in Table 3.

Summary and conclusions

Five different radiosonde packages were deployed during the 2004 NSA experiment conducted at the ARM's Great White field site near Barrow, Alaska, during March 9-April 9, 2004. Comparisons between temperature and relative humidity profiles have been presented, as well as comparisons in PWV between data taken by the ARM Microwave Radiometer and Microwave Profiler, the Global Positioning Systems, and each of the various radiosonde types. Our conclusions can be summarized as follows:

(1) Relative humidity measurements from the VIZ carbon hygristor (both the NWS-VIZ and the SW-CH) show an apparent bias with respect to the other instruments above the troposphere, with an average bias of the order of 16-20%. The CH measurements have also shown less accuracy in the RH measurements, which could be due to the time lag and response time of the instruments.

(2) Conversely, the Vaisala H-Humicap and the Snow White chilled mirror have shown good agreement in the RH measurements, with an average value of 0.5% and an average rms difference of the entire profile of the order of 5%. Still, the presence of some spikes in the measurements, which may be associated with the switching between the two humidity elements, should be further investigated.

(3) GPS measurements taken at Barrow provided the general pattern of PWV, in particular during cloudy or snowy conditions, and the continuous availability (every 30-minutes) is very useful. However, NRT data are affected by a substantial scatter compared to the MWRs. Reprocessing reduced most but not all this scatter, as shown in the comparison with the MWR and the MWRP, where occasional GPS differences exceeded 1 mm when PWV values were less than 1 cm.

(4) The PWV retrieved from the MWRP by using 2 channels (22.235 and 30 GHz) does not provide PWV values with the required accuracy, due to a less frequent sampling of each channel of the profiler with respect to the MWR. The use of the available five channels in the water vapor band provides very good agreement with the MWR, with less than 0.035 cm rms. PWV retrieved by using 6 channels (five K-band channel and the 51.25 GHz) has also been considered. The retrieval produces similar results as the 5-channel retrieval, with an rms difference of the order of 0.015 cm, and a slightly better agreement of the 6-channel with the MWR.

(5) The use of remote sensing data to identify spurious radiosonde data was especially useful, and should be considered in automated quality control.

(6) There was an unexplained bias in night-time temperature soundings above 10 km between the NWS and Duplex soundings. This bias reached about 5ºC at 20 km. The once-a-day soundings at the Great White were not sufficient to study further this bias.

(7) Oversample sizes that ranged from about 1000 to 7000 data points, the GPS, MWR, and MWRP (5-channel) PWV retrievals data were consistent with biases 0.03 cm, std less than 0.05, and regression slopes better than 0.98.

(8) The possibility of diurnal differences in the data is still being investigated. However, is clear to us that to increase the once-a-day sounding at the Great White to twice a day would be of substantial benefit to a variety of studies.

Acknowledgements

The work presented in this paper was sponsored by the Environmental Sciences Division of the Department of Energy as a part of their Atmospheric Radiation Measurement Program.
The authors wish to thank Janet Machol for her useful comments on the manuscript.

Corresponding Author

Vinia Mattioli, vinia.mattioli@diei.unipg.it, (011-39) 075-585-3660

References

Bevis, M, S Businger, S Chiswell, T Herring and R Anthes, 1994: GPS meteorology-mapping zenith wet delays onto precipitable water, J Appl Meteorology, 33(3), 379-386.

Cimini, D., A. J. Gasiewski, M. Klein, E.R. Westwater, V. Leuski, and S. Dowlatshahi, 2005: Ground-based Scanning Radiometer Measurements during the Water Vapor IOP 2004: a valuable new data set for the study of the Arctic atmosphere. *Proc. of the 15th ARM Science Team Meeting*, March 14-18, Daytona Beach, Florida.

Clough, S. A., P. D. Brown, D. D. Turner, T. R. Shippert, J. C. Liljegren, D. C. Tobin, H. E. Revercomb, and R.O. Knuteson, 1999: Effect on the Calculated Spectral Surface Radiances Due to MWR Scaling of Sonde Water Vapor Profiles. *Proc. of the 9th Atmospheric Radiation Measurement (ARM) Science Team Meeting*, U.S. Department of Energy, Washington, D.C. [Available URL: http://www.arm.gov/publications/proceedings/conf09/abstracts/clough-99.pdf].

Gutman, S.I., S.R. Sahm, S.G. Benjamin, B.E. Schwartz, K.L. Holub, J.Q. Stewart, and T.L. Smith, 2004a: Rapid Retrieval and Assimilation of Ground Based GPS Precipitable Water Observations at the NOAA Forecast Systems Laboratory: Impact on Weather Forecasts. Journal of the Meteorological Society of Japan, Vol. 82, No. 1B, pp. 351-360.

Gutman, S.I., S.R. Sahm, S.G. Benjamin, T.L. Smith, 2004b: GPS water vapor observation errors. 8th Eighth Symposium on Integrated Observing and Assimilation Systems for Atmosphere, Oceans, and Land Surface, paper 8.3, Seattle, WA Jan. 11-15.

Fujiwara, M., M. Shiotani, F. Hasebe, H. Voemel, S. J. Oltmans, P. W. Ruppert, T. Horinouchi, and T. Tsuda, 2003: Performance of the Meteolabor "Snow White" chilled-mirror hygrometer in the tropical troposphere: Comparisons with the Vaisala RS80 A/H-Humicap sensors. *J. Atmos. Ocean. Technol.*, 20, 1534–1542.

Han, Y. and Westwater E.R., 2000: Analysis and improvement of tipping calibration for ground-based microwave radiometers. *IEEE Trans. Geosci. Remote Sensing*, 38, 1260-1276.

King, R.W. and Y. Bock. 1996: Documentation of the GAMIT GPS analysis software, version 9.4. Massachusetts Institute of Technology and Scripps Institution of Oceanography.

Liljegren, J. C. 2000: Automatic self-calibration of ARM microwave radiometers. *Microwave Radiometry and Remote Sensing of the Earth's Surface and Atmosphere*. Utrecht: P. Pampaloni and S. Paloscia, Eds., VSP Press, 433–443.

Liljegren, J. C. and B.M. Lesht, 2004: Preliminary results with the twelve-channel Microwave Radiometer Profiler at the North Slope of Alaska Climate Research Facility. *Proc. of 14th ARM Science Team Meeting*. March 22-26, 2004, Albuquerque, New Mexico. [Available on-line at: http://www.arm.gov/publications/proceedings/conf14/extended_abs/liljegren-jc.pdf]

Liljegren, J. C., S. –A Boukabara, K. Cady-Pereira, and S. A. Clough, 2005: The Effect of the Half-Width of the 22-GHz Water Vapor Line on Retrievals of Temperature and Water Vapor Profiles with a Twelve-Channel Microwave Radiometer. *IEEE Trans. Geosci. Remote Sensing,* 43 (5), 1102-1108.

Mattioli, V., E. R. Westwater, S. I. Gutman, and V. R. Morris, 2005: Forward Model Studies of Water Vapor using Scanning Microwave Radiometers, Global Positioning System, and Radiosondes during the Cloudiness Inter-Comparison Experiment. *IEEE Trans. Geosci. Remote Sensing*, 43 (5), 1012-1021.

National Weather Service, Office of Systems Operations, 1999: Environmental chamber tests of NWS radiosonde relative humidity sensors. *1999 American Meteorological Society Conference, 15th International Conference on Interactive Information and Processing Systems (IIPS)*, Dallas, TX, January 10–15. [Available at: http://www.ua.nws.noaa.gov/paper-1.htm].

Paukkunen, A., V. Antikainen, H. Jauhiainen, 2001: The accuracy and performance of the new Vaisala RS90 radiosonde in operational use. *11th Symposium on Meteorological Observations and Instrumentation, 81st AMS Annual Meeting*, January 14-19, Albuquerque, NM.

Racette, E. P., E. R. Westwater, Y. Han, A. J. Gasiewski, M. Klein, D. Cimini, D. C. Jones, W. Manning, E. J. Kim, J. R. Wang, V. Leuski, and P. Kiedron, 2005: Measurement of Low Amounts of Precipitable Water Vapor Using Ground-Based Millimeterwave Radiometry. *J. Atmos. Ocean. Tech*., 22 (4), 317 – 337.

Revercomb H. E., D. D. Turner, D. C. Tobin, R. O. Knuteson, W. F. Feltz, J. Bannard, J. Bosenberg, S. Clough, D. Cook, R. Ferrare, J. Goldsmith, S. Gutman, R. Halthorne, B. Lesht, J. Liljegren, H. Linne, J. Michalsky, V. Morris, W. Porch, S. Richardson, B. Schmid, M. Splitt, T. Van Hove, E. Westwater, and D. Whiteman, 2003: The ARM programs's water vapor intensive observation periods: overview, initial accomplishments, and future challenges. *Bull. Amer. Meteorol. Soc.* 217-236.

Saastamoinen, J., 1972. Introduction to practical computation of astronomical refraction, Bull. Geod., 106, 383-397.

Voemel, H., M. Fujiwara, M. Shiotani, F. Hasebe, S. J. Oltmans, and J. E. Barnes, 2003: The behavior of the Snow White chilled-mirror hygrometer in extremely dry conditions. *J. Atmos. Ocean. Technol.*, 20, 1560–1567.

Wang, J., H. L. Cole, D. J. Carlson, E. R. Miller, K. Beierle, A. Paukkunen, and T. K. Laine, 2002: Correction of humidity measurement errors from the Vaisala RS80 radiosonde-Application to TOGA COARE data. *J. Atmos. Ocean. Technol*., 19, 981–1002.

Wang, J., D. J. Carlson, D. B. Parsons, T. F. Hock, D. Lauritsen, H. L. Cole, K. Beierle, and E. Chamberlain, 2003: Performance of operational radiosonde humidity sensors in direct comparison with a chilled mirror dew-point hygrometer and its climate implication. *Geophys. Res. Lett.*, 30 (16), 1860, 10.1029/2003GL016985.

Westwater, E. R., B. Stankov, D. Cimini, Y. Han, J. A. Shaw, B. M. Lesht, and C. N. Long, 2003: Radiosonde Humidity Soundings and Microwave Radiometers during Nauru99. *J. Atmos. Ocean. Tech*, 20 (7), 953-971.

Westwater, E.R., Klein, M., Gasiewski, A., Leuski, V., Shaw, J.A., Mattioli, V., Cimini, D., Liljegren, J.C., Lesht, B.M., Zak, B.D., Uttal, T., Hazen, D.A., Weber, B.L., and Dowlatshahi, S., 2004: The 2004 North Slope of Alaska Arctic Winter Radiometric Experiment. *Proc. of 14th ARM Science Team Meeting*. March 22-26, 2004, Albuquerque, New Mexico. [Available on-line at: http://www.arm.gov/publications/proceedings/conf14/extended_abs/westwater-er.pdf].

Westwater, E. R., D. Cimini, V. Mattioli, M. Klein, V. Leuski, A. J. Gasiewski, S. Dowlatshahi, J. S. Liljegren, B. M. Lesht, and J. A. Shaw, 2005: Microwave and Millimeter Wave Forward Modeling Results from the 2004 North Slope of Alaska Arctic Winter Radiometric Experiment. *Proc. of the 15th ARM Science Team Meeting***,** March 14-18, Daytona Beach, Florida.

FIGURES AND TABLES

Table 1: Geographical position of the RAOB stations.

	Latitude (degrees)	Longitude (degrees)	Height (m)
ARM Duplex	71.33 N	156.68 W	8
ARM Great White	71.32 N	156.62 W	8
NWS Station	71.30 N	156.78 W	12

Table 2. Number of soundings deployed and available after the processing. The number of outliers for each radiosonde type, identified after intercomparisons among the RAOBs and with remote sensing instruments (GPS, MWR, MWRP), is given in parentheses.

RAOBs type	N. launches	Post-processed soundings
DPLX-RS90 sondes	124	114 (1)
GW-RS90 sondes	28	26 (0)
SW sondes	10	8 (0)
NWS-VIZ sondes	51	48 (4)

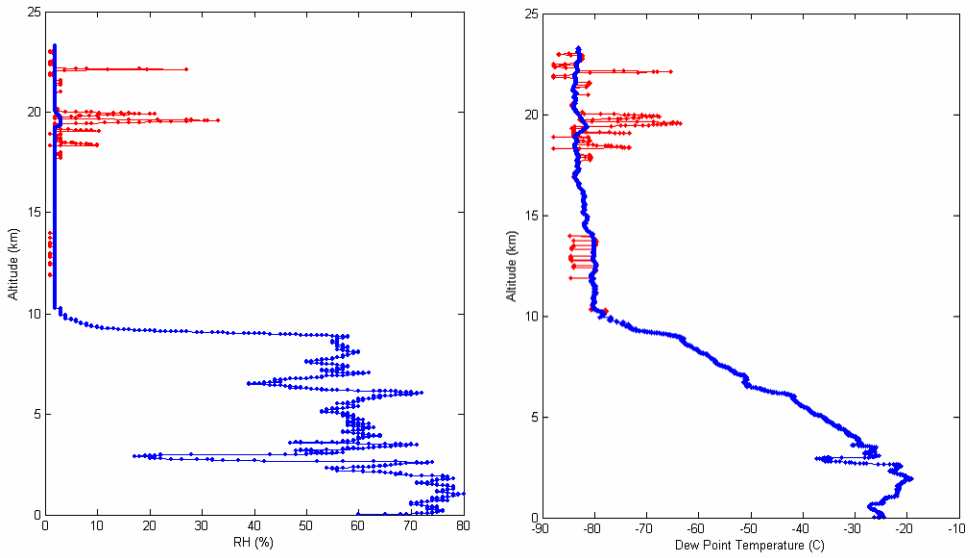

Figure 1. Relative humidity and dew-point temperature affected by unrealistic noise (red dots) and reconstructed profiles (blue dots) in the DPLX-RS90 sounding launched on April 4, 2004, at 2300 UTC. Here, the first spurious data occur at about 12 km.

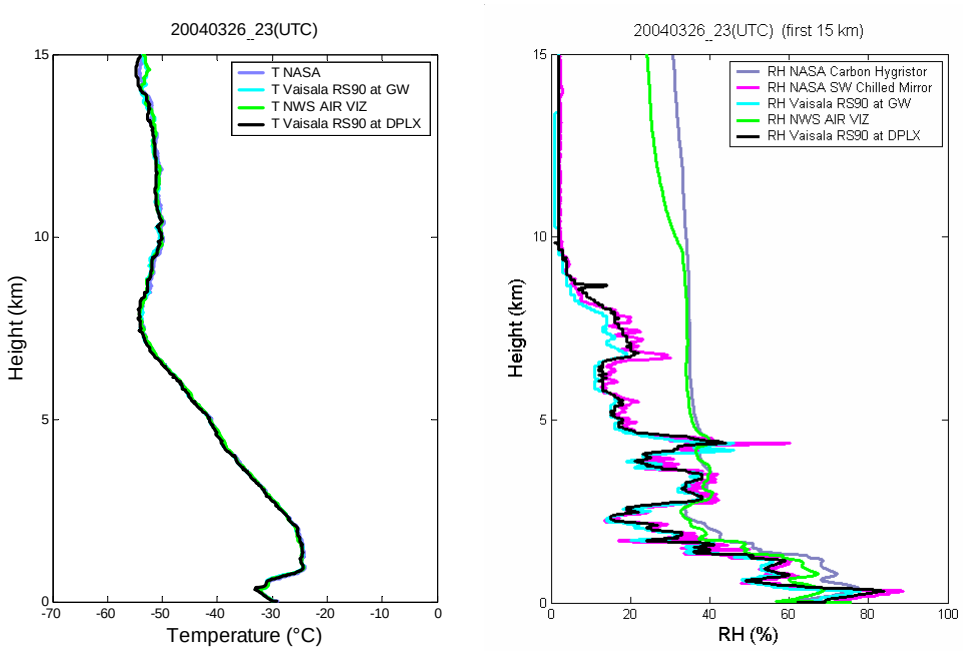

Figure 2. Temperature (left) and relative humidity (right) soundings on March 26 at 2300 UTC.

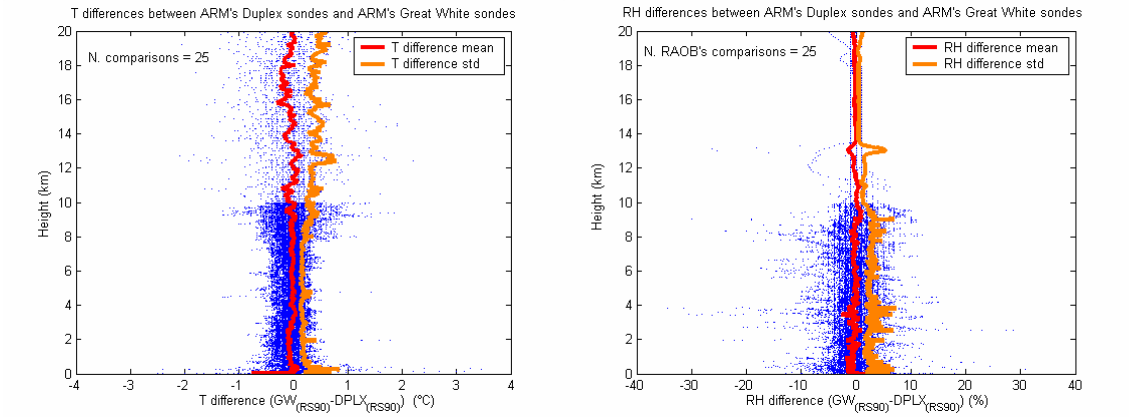

Figure 3. T difference profiles (left) and RH difference profiles (right) between the Vaisala RS90 radiosondes launched at the DPLX and at the GW. Level 2.0 data were used for the comparison. Since the interpolating grid in altitude is 10 m below 10 km and 100 m above it, the points below 10 km are denser than above 10 km.

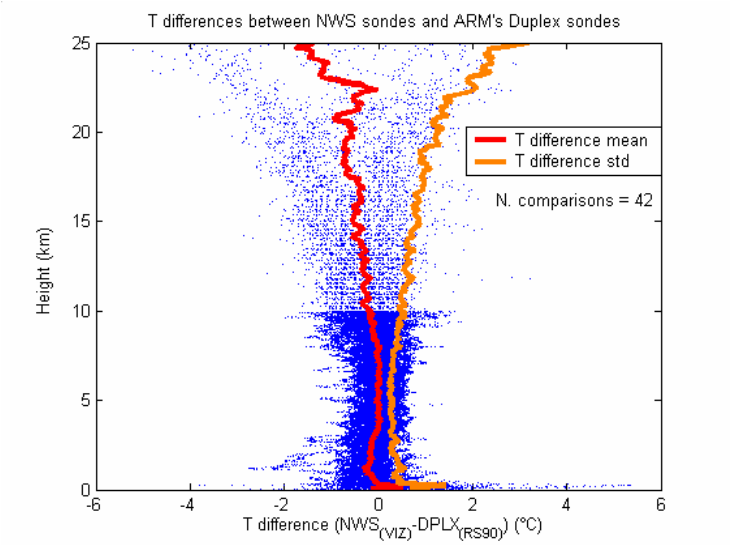

Figure 4. Temperature difference profiles between the NWS-VIZ and the DPLX-RS90 radiosondes.

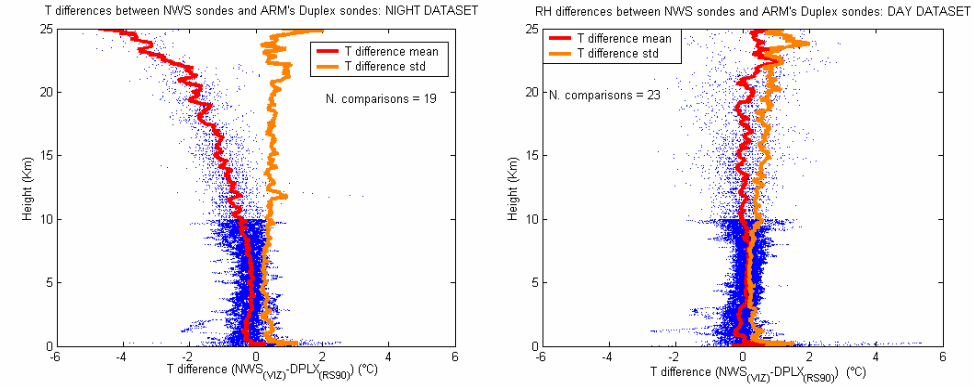

Figure 5. T difference profiles between the NWS-VIZ radiosondes and the DPLX-RS90. (left) Dataset taken at night (1100 UTC, 2 a.m. local time), (right) dataset taken during the day (2300 UTC, 2 p.m. local time).

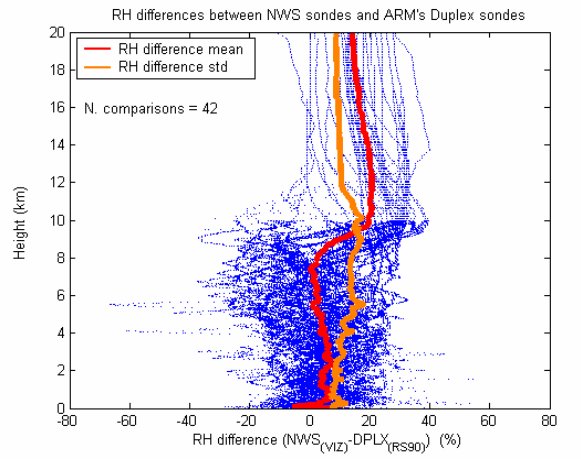

(a)

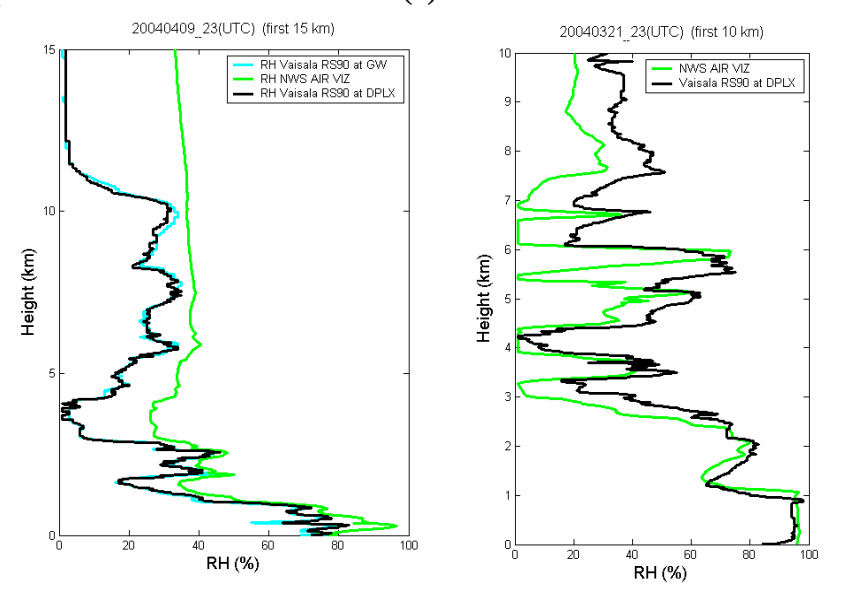

(b) (c)

Figure 6. (a) RH difference profiles between the NWS-VIZ radiosondes and the DPLX-RS90. (b) Soundings taken on April 9, at 2300 UTC. (c) Soundings taken on March 21, at 2300 UTC.

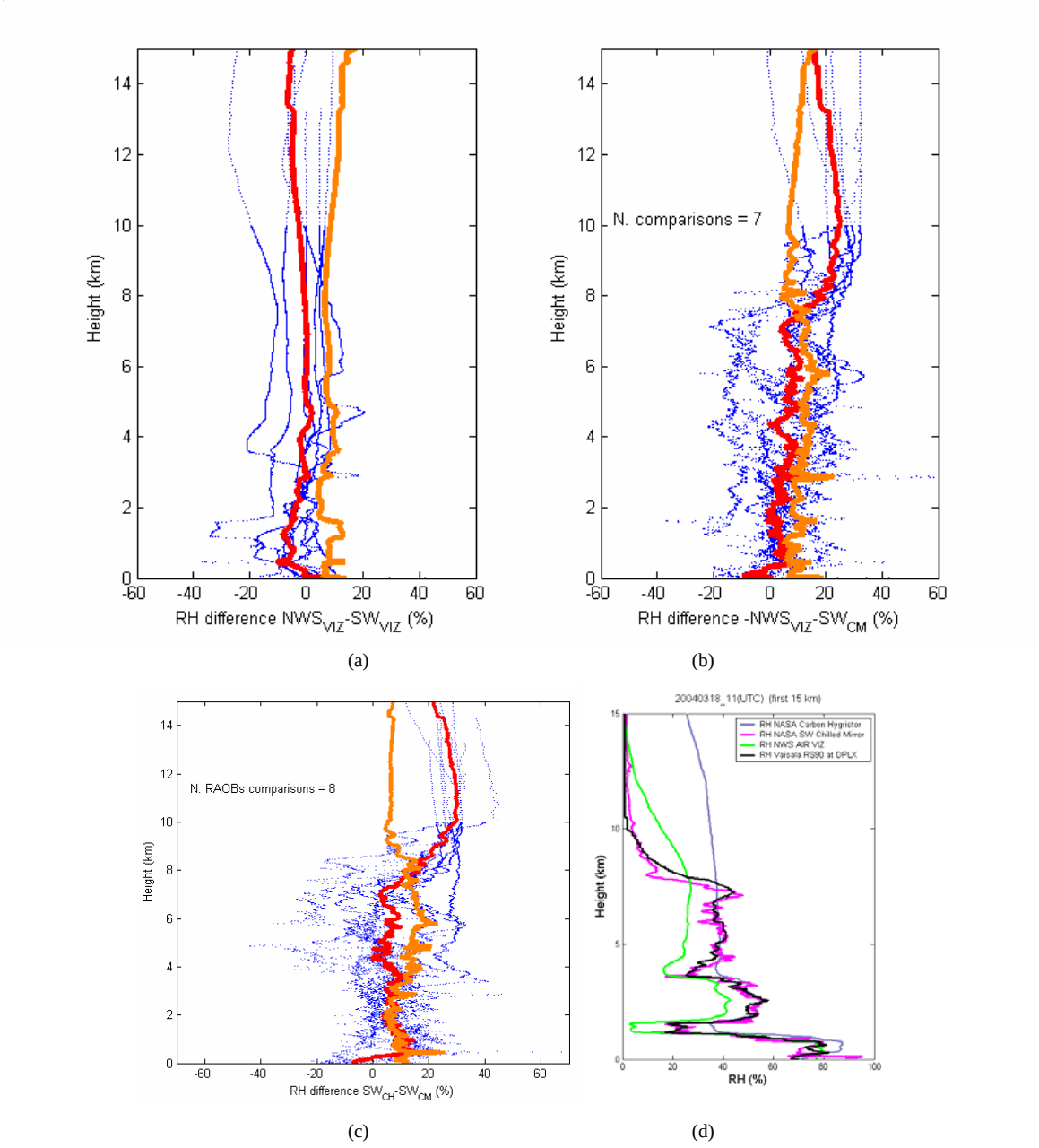

Figure 7. Profiles of RH difference between the carbon hygristor and chilled mirror: (a) NWS-VIZ vs. SW-CH, (b) NWS-VIZ vs. SW-CM, (c) SW-CH vs. SW-CM. (d) Relative humidity soundings taken on March 18, at 1100 UTC.

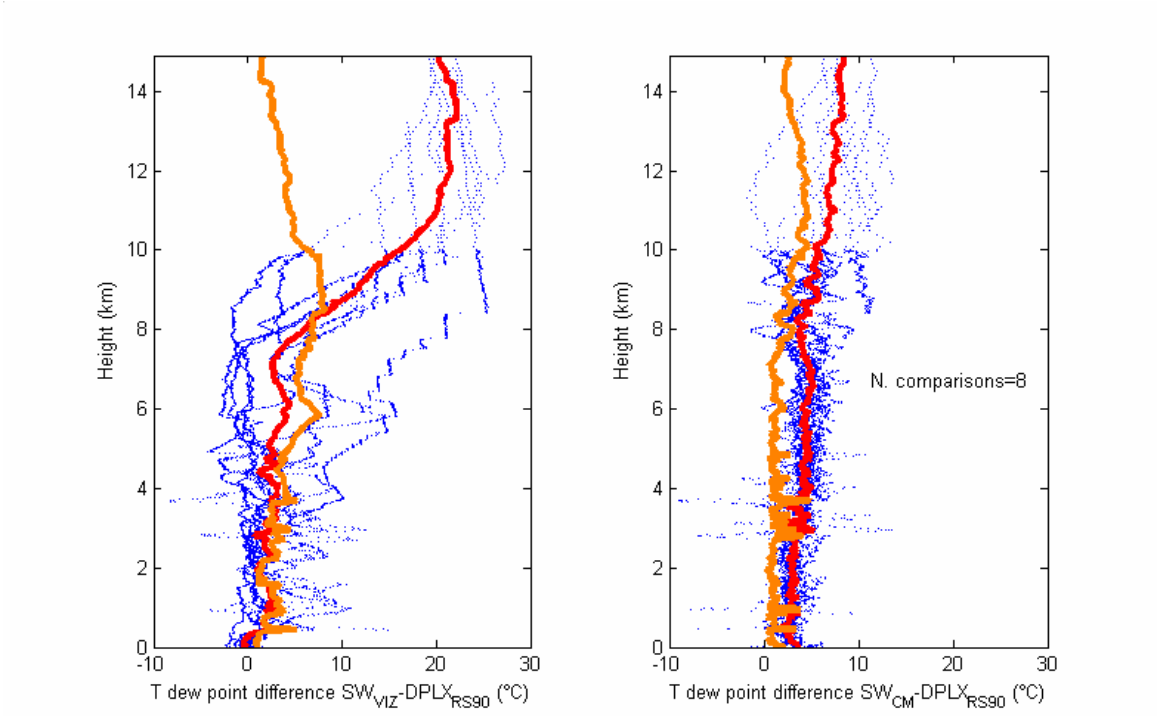

Figure 8. RH difference profiles between the NASA sensors SW-CH (left), SW-CM (right), and the Vaisala RS90 H-Humicap operated at the Duplex.

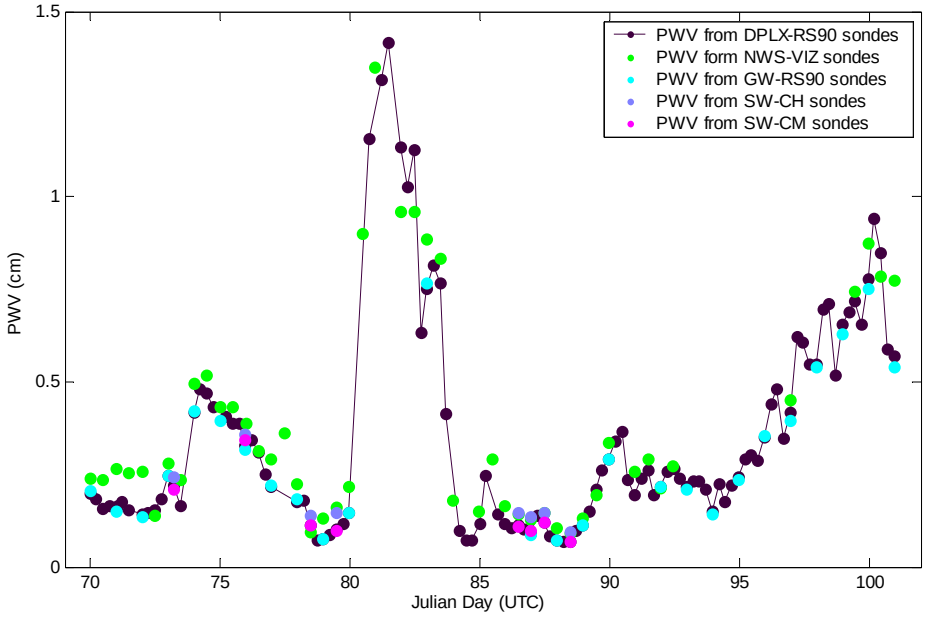

Figure 9. PWV time series computed from the radiosondes that were operating during the 2004 NSA experiment.

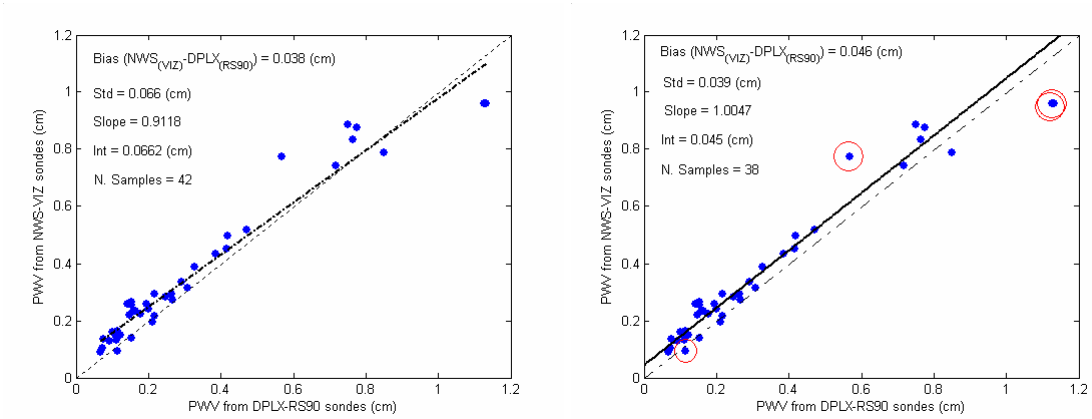

Figure 10. PWV from NWS-VIZ compared with PWV from the DPLX-RS90: all data of the experiment (left), all data with four soundings removed (right). Outliers are enclosed in red circles.

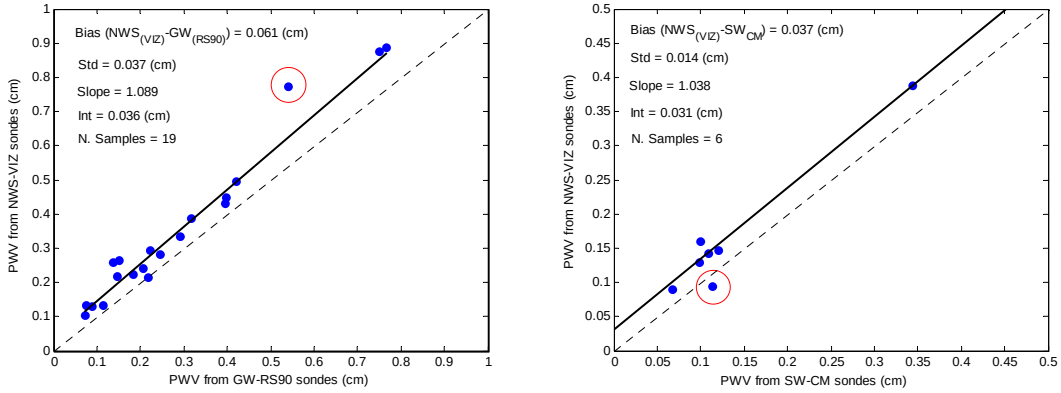

Figure 11. PWV from NWS-VIZ compared to PWV from GW-RS90 (left), and compared to PWV from SW-CM (right). Outliers are removed from the statistics and shown in the scatterplot enclosed in red circles.

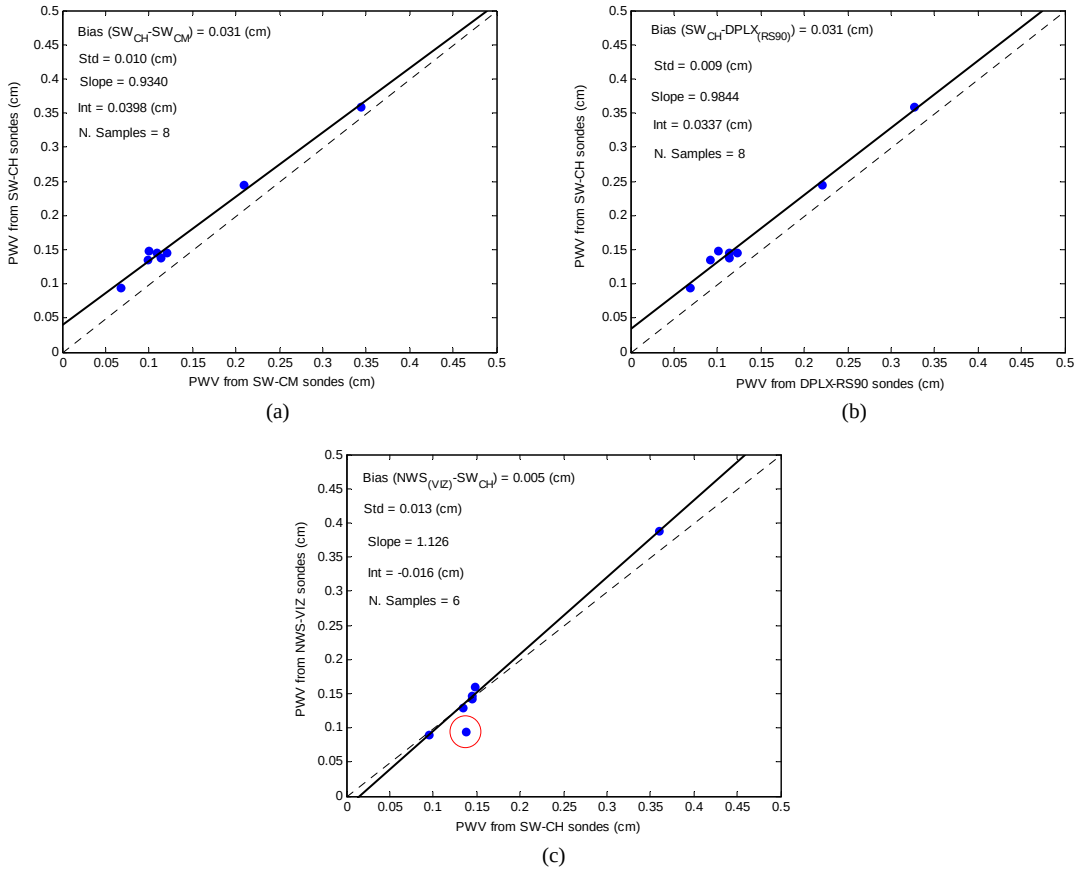

Figure 12. Comparison of PWV from the SW-CH: (a) with the PWV from the SW-CM, (b) with the PWV from the DPLX-RS90, (c) with PWV from the NWS-VIZ radiosonde. The outlier is removed from the statistics and shown in the scatterplot enclosed in red circle.

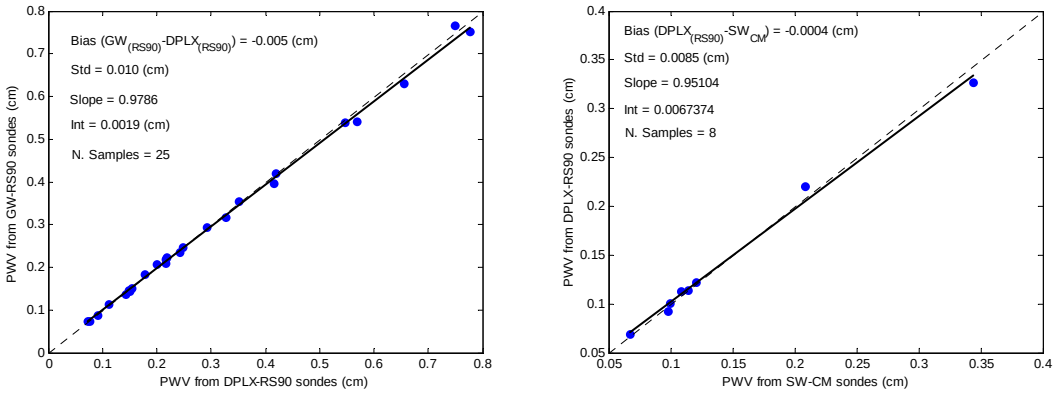

Figure 13. (Left) PWV from the GW-RS90 compared with PWV from the DPLX-RS90. (Right) PWV from the DPLX-RS90 compared with PWV from the SW-CM.

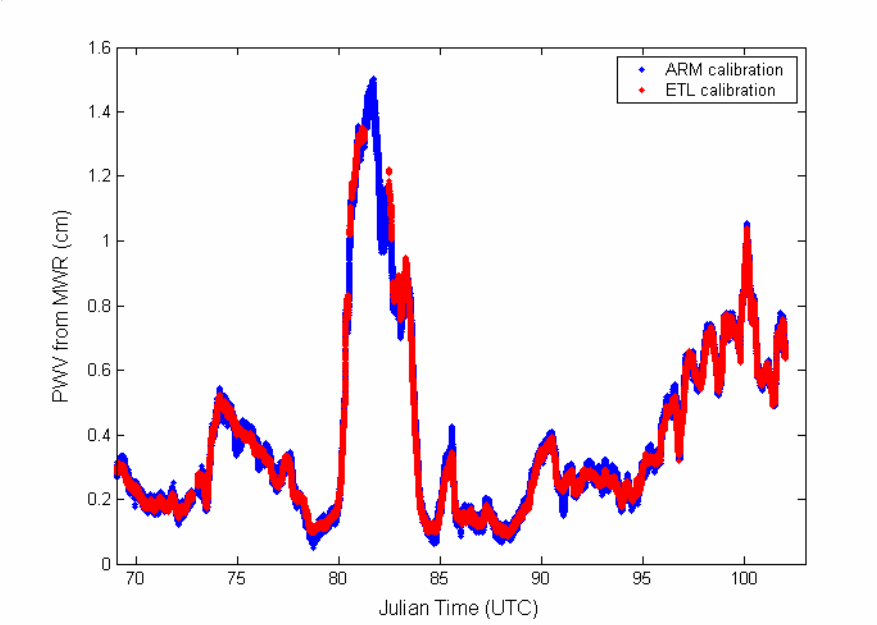

Figure 14. PWV derived from the MWR using the ETL and the ARM calibration algorithms

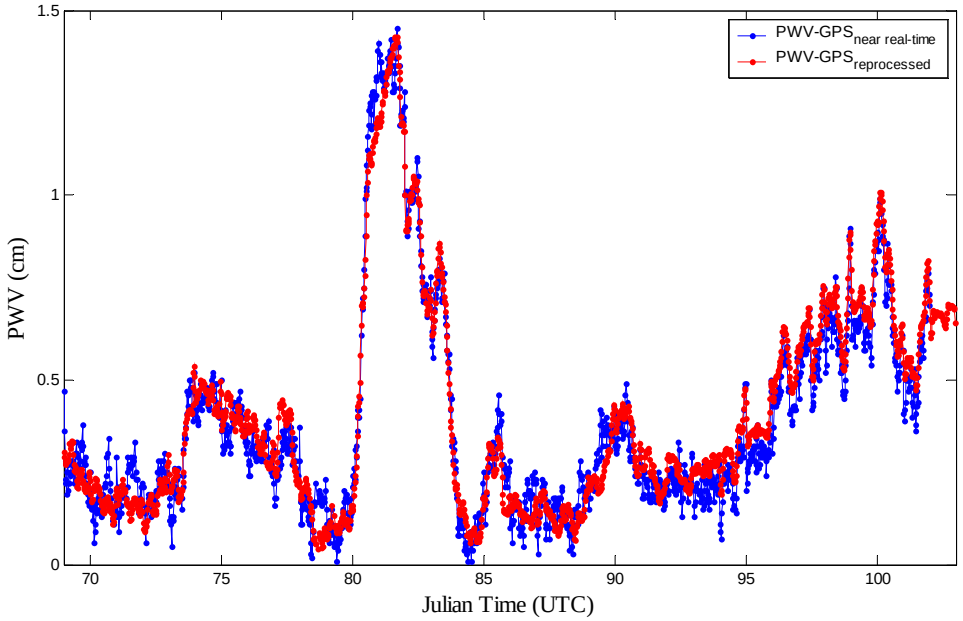

Figure 15. PWV time series of the GPS near real-time (blue) and reprocessed (red) data.

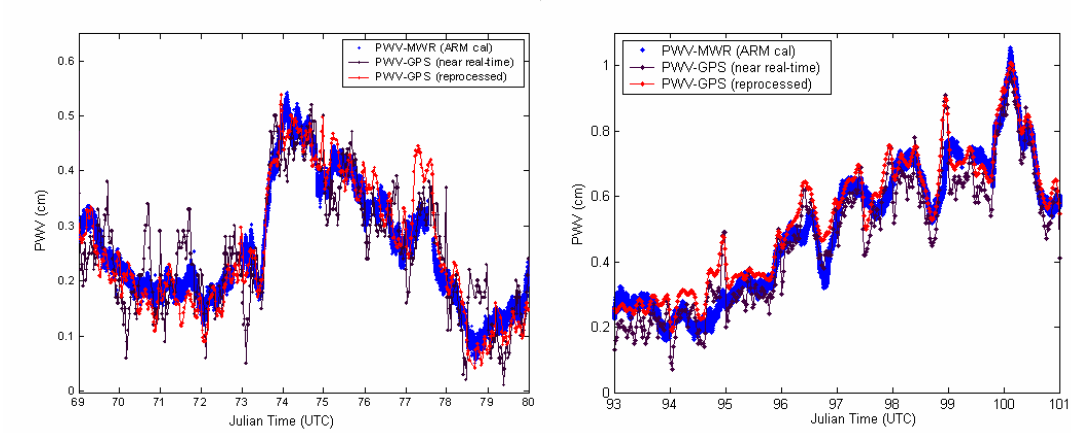

Figure 16. PWV time series from the MWR (blue dots), the near real-time GPS data (black dots), and reprocessed GPS data (red dots): (left) March 9-20, 2004, (right) April 4-9, 2004.

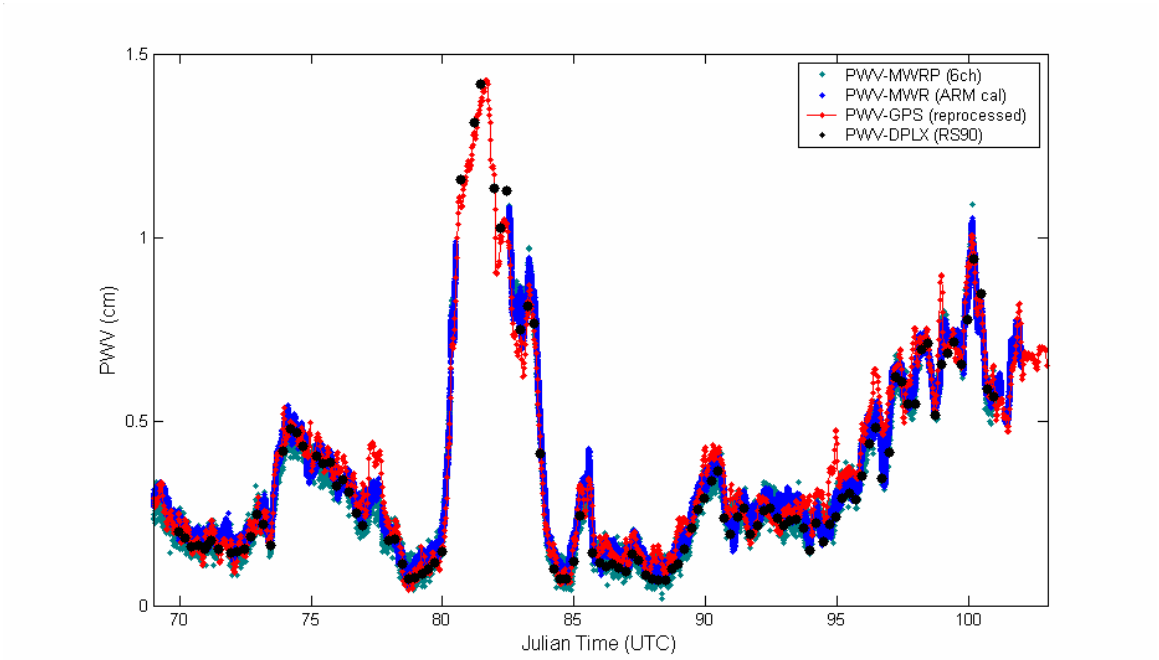

Figure 17. PWV time series of PWV from the MWRP, retrieved by using 6 channels, from the MWR, ARM calibration applied, the reprocessed GPS and the DPLX-RS90 radiosondes.

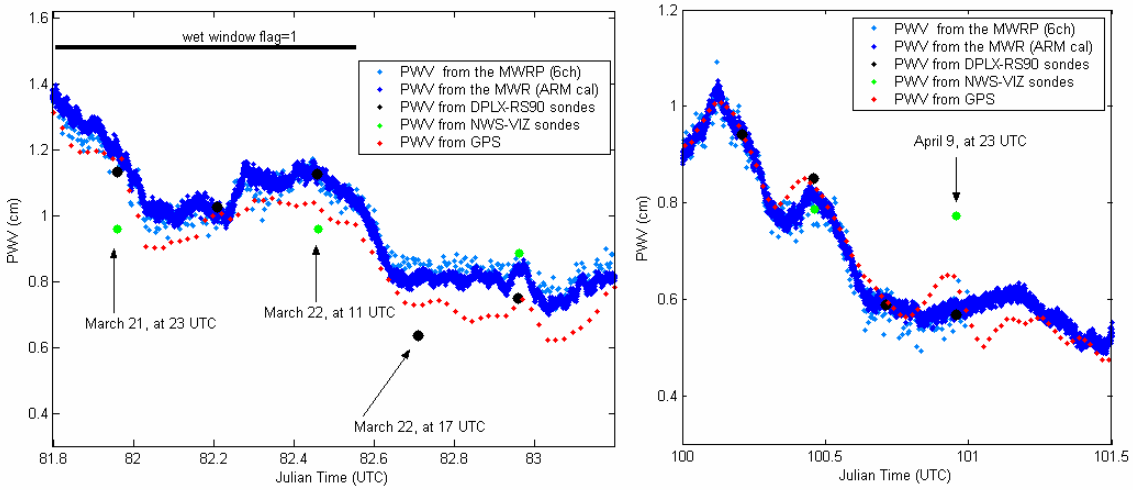

Figure 18. PWV time series from the MWRP, the MWR, the GPS and the DPLX-RS90 and NWS-VIZ radiosondes. Radiosonde outliers are indicated by the arrows.

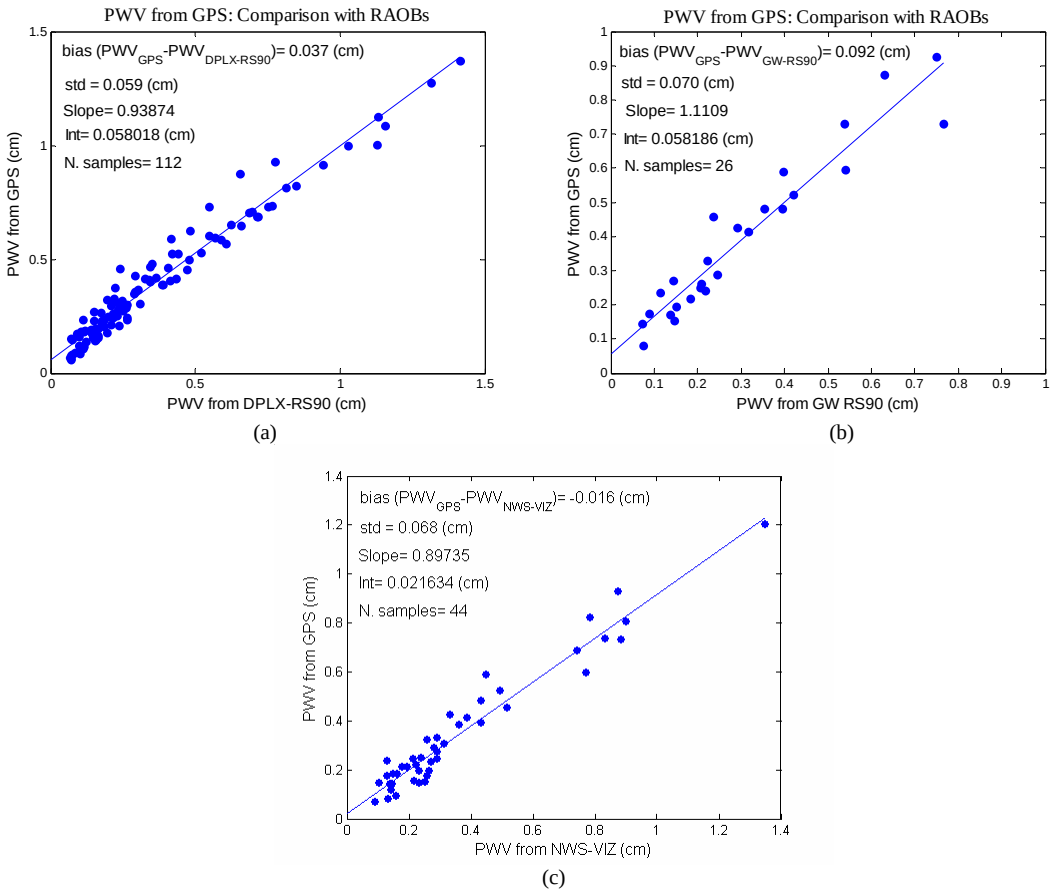

Figure 19. PWV from the radiosondes compared with GPS: (a) PWV from GPS compared with the DPLX-RS90, (b) PWV from GPS compared with the GW-RS90, (c) PWV from GPS compared with the NWS-VIZ radiosondes.

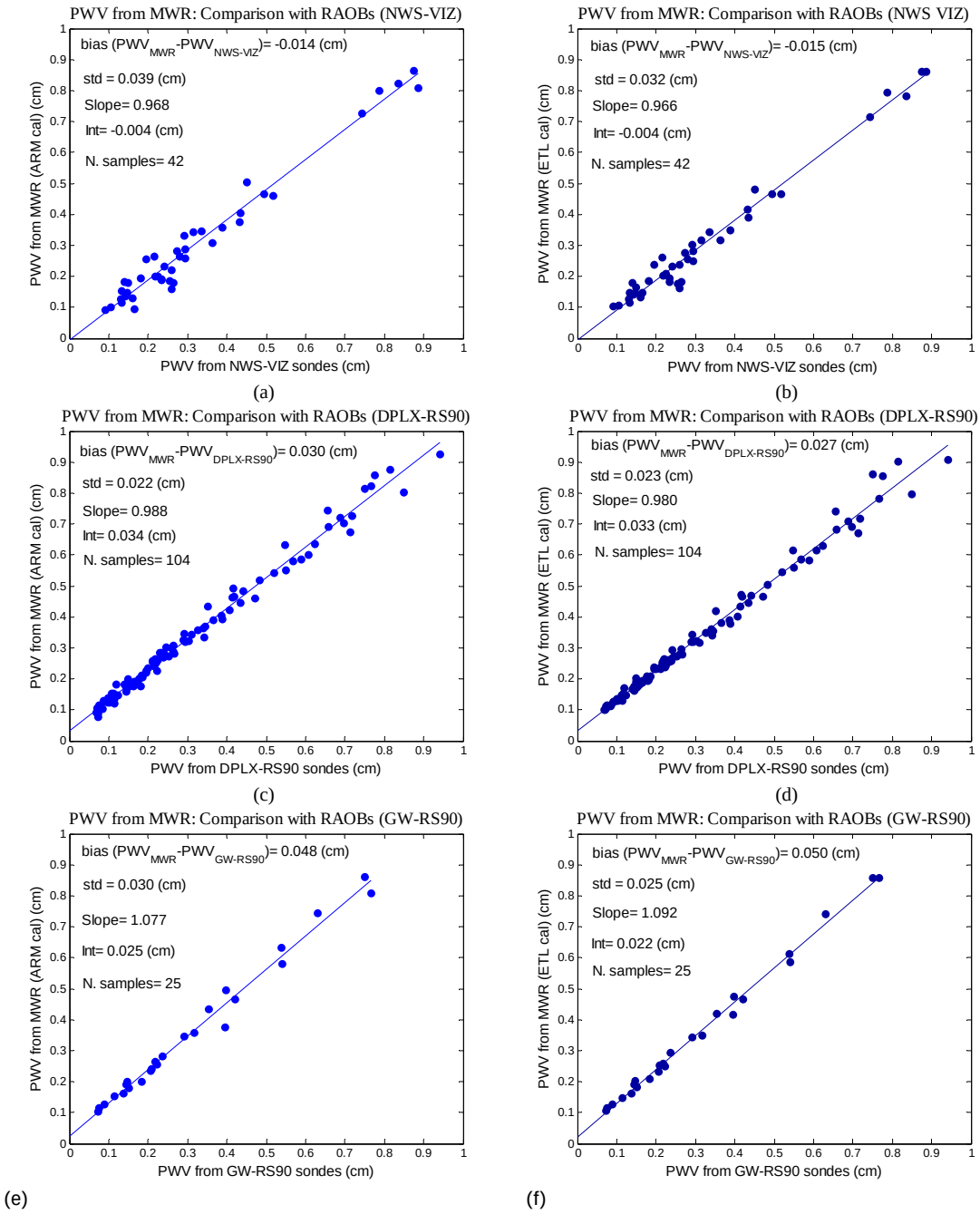

Figure 20. PWV from MWR compared with PWV from the radiosondes: (a) MWR (ARM calibration applied) compared with the NWS-VIZ radiosondes, (b) MWR (ETL calibration applied) compared with the NWS-VIZ radiosondes, (c) MWR (ARM calibration applied) compared with the DPLX-RS90, (d) MWR (ETL calibration applied) compared with the DPLX-RS90, (e) MWR (ARM calibration applied) compared with the GW-RS90, (f) MWR (ETL calibration applied) compared with the GW-RS90.

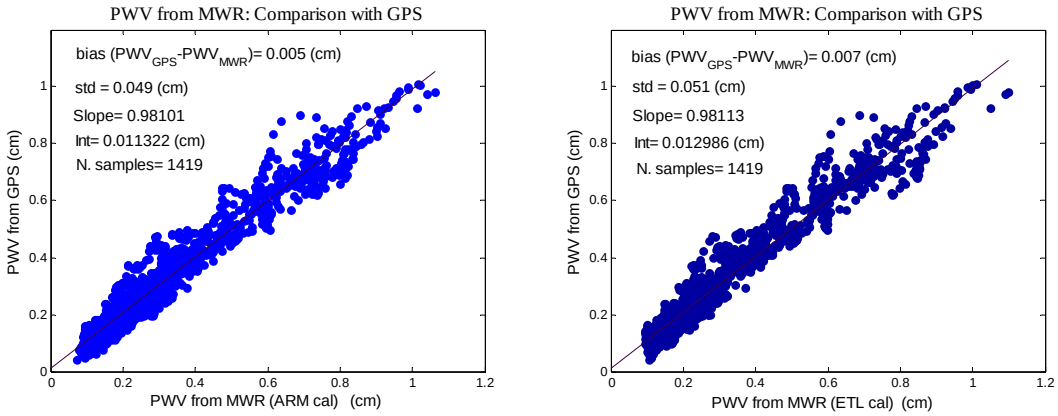

Figure 21. (Left) PWV from GPS compared with PWV from MWR (ARM calibration); (right) PWV from GPS compared with PWV from MWR (ETL calibration).

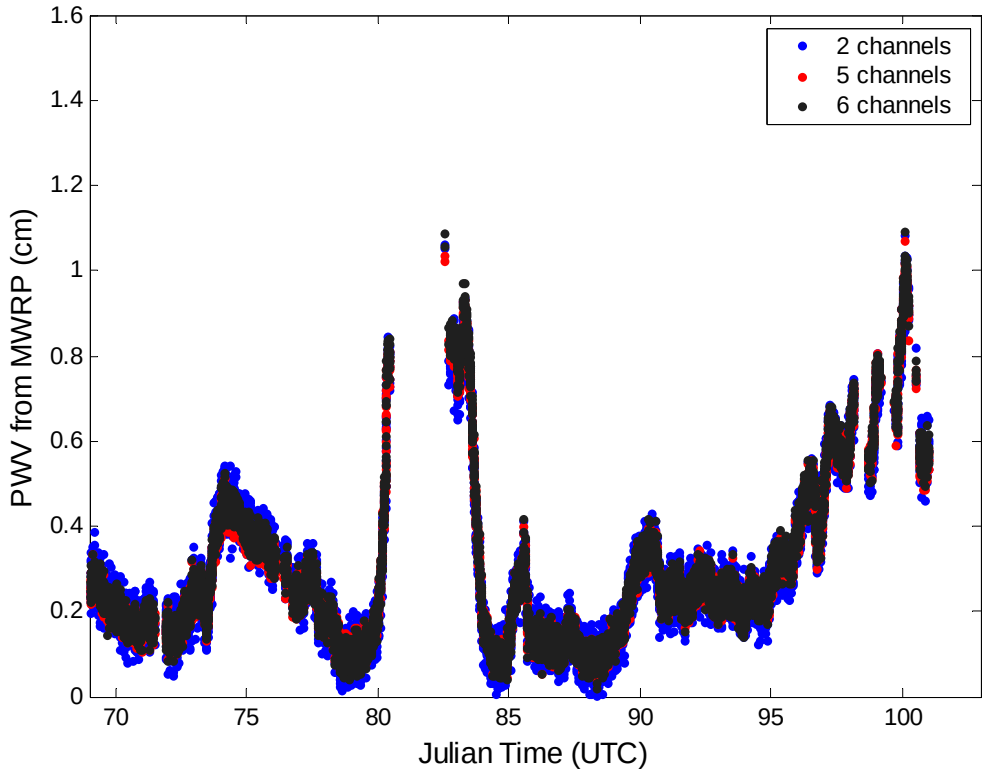

Figure 22. PWV time series from the MWRP, by using two-channel retrieval (blue dots), five-channel retrieval (red dots), and 6-channel retrieval (black dots).

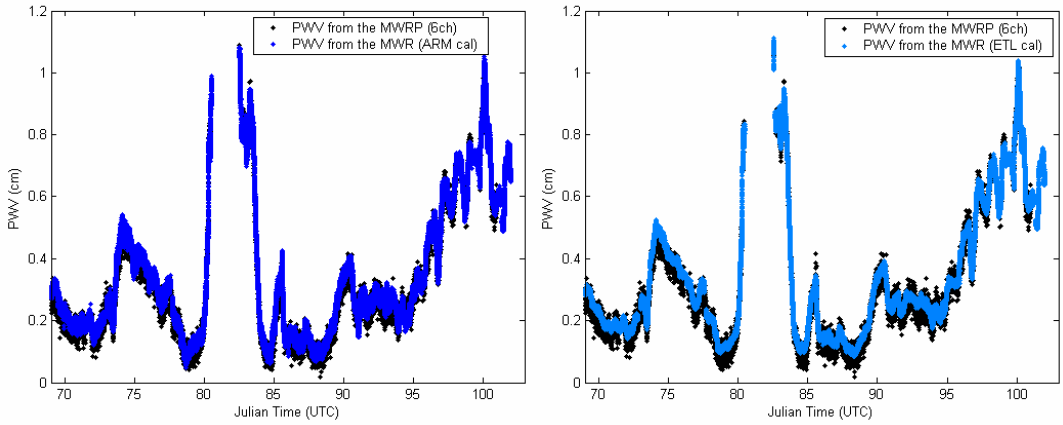

Figure 23. PWV from MWRP (black dots) retrieved from 6 channels, and PWV from the MWR, ARM calibration (blue dots), and ETL calibration (cyan dots). .

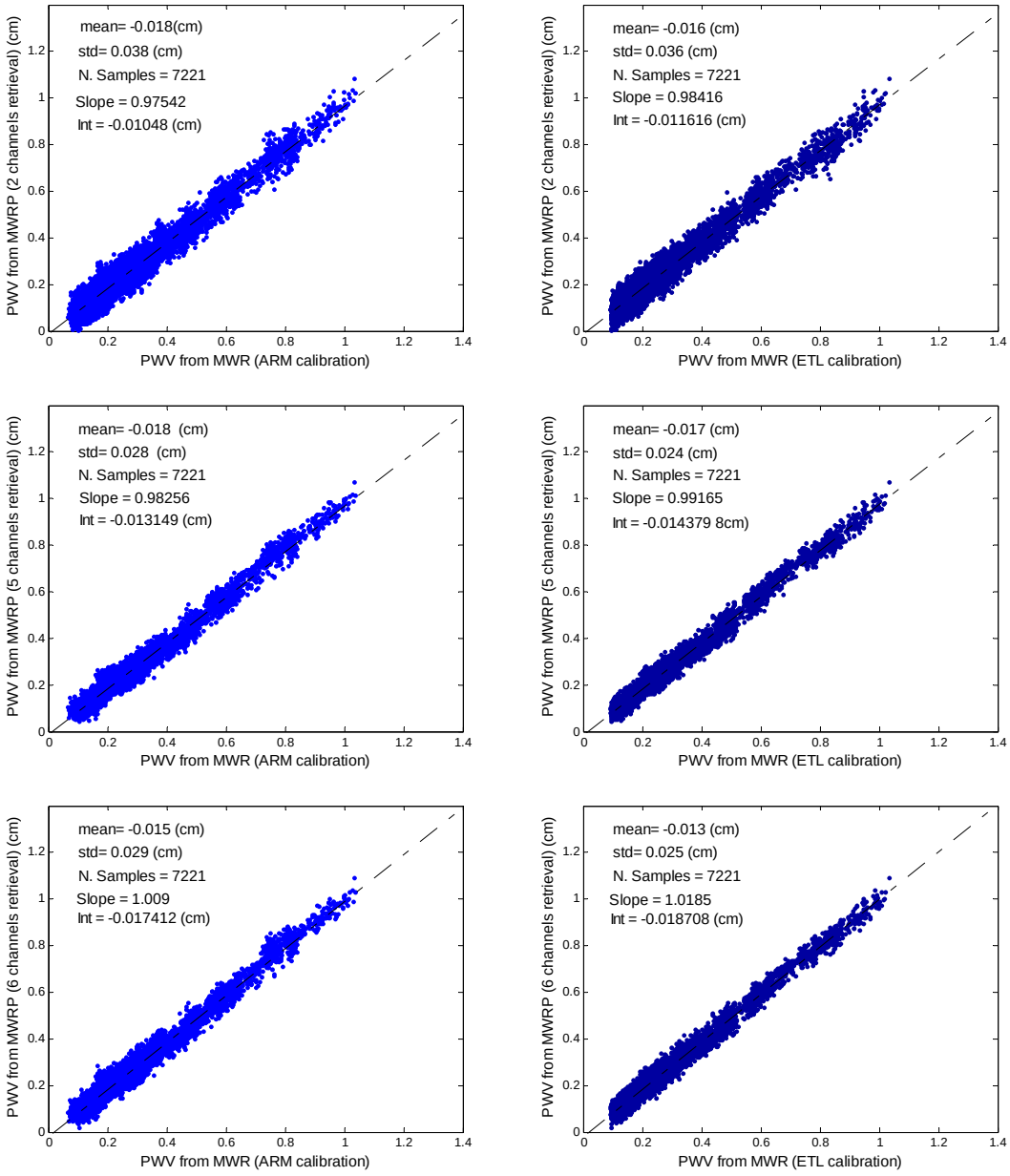

Figure 24. PWV from MWRP retrieved using 2 channels (top), 5 channels (middle) and 6 channels (bottom) compared with PWV from MWR, ARM calibration (right) and ETL calibration (left). Mean values refer to (MWRP-MWR).

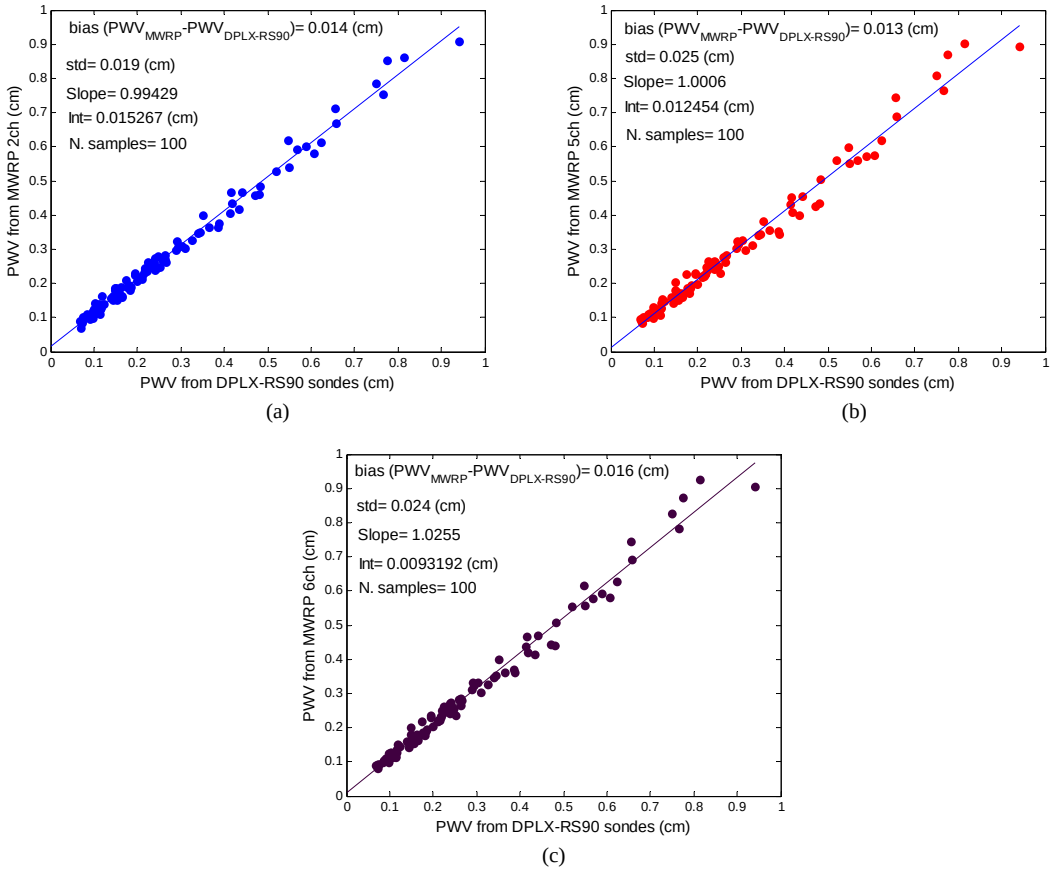

Figure 25. PWV from the MWRP compared with PWV from the DPLX-RS90 sondes: (a) comparison for the MWRP 2-channel retrieval, (b) for the 5-channel retrieval, (c) for the 6-channel retrieval.

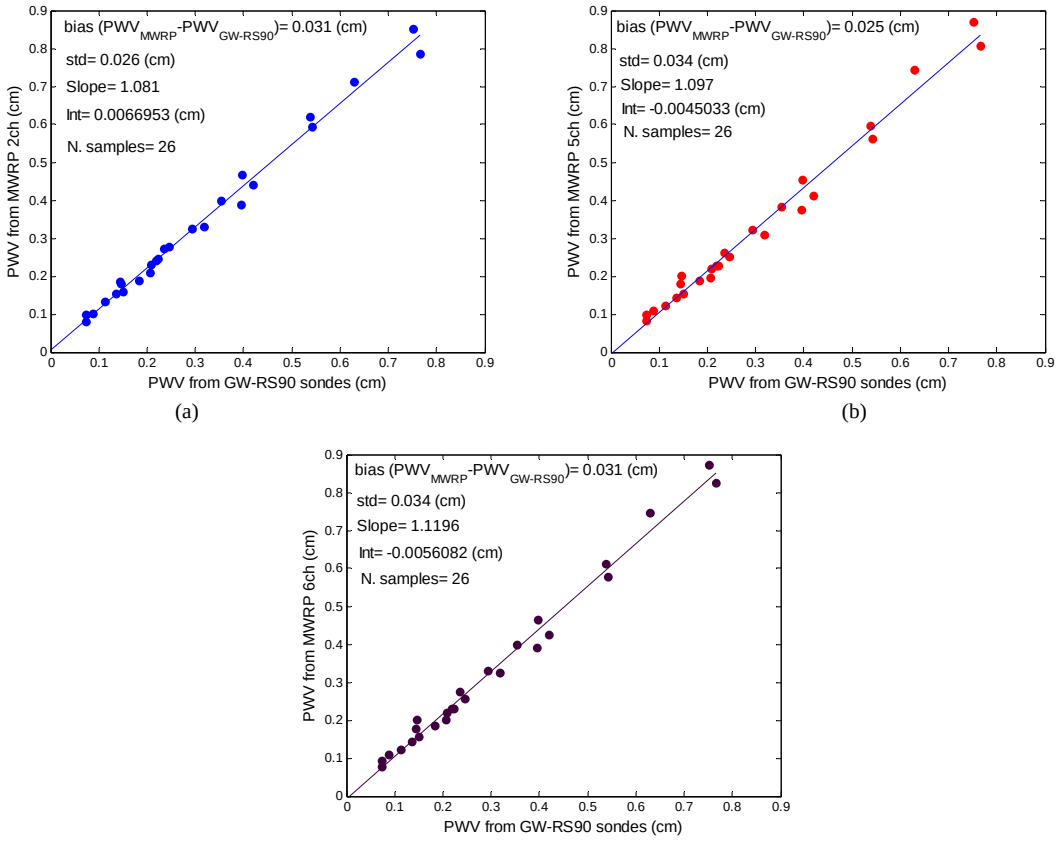

Figure 26. PWV from the MWRP compared with PWV from the GW-RS90 sondes: (a) comparison for the MWRP 2-channel retrieval, (b) for the 5-channel retrieval, (c) for the 6-channel retrieval.

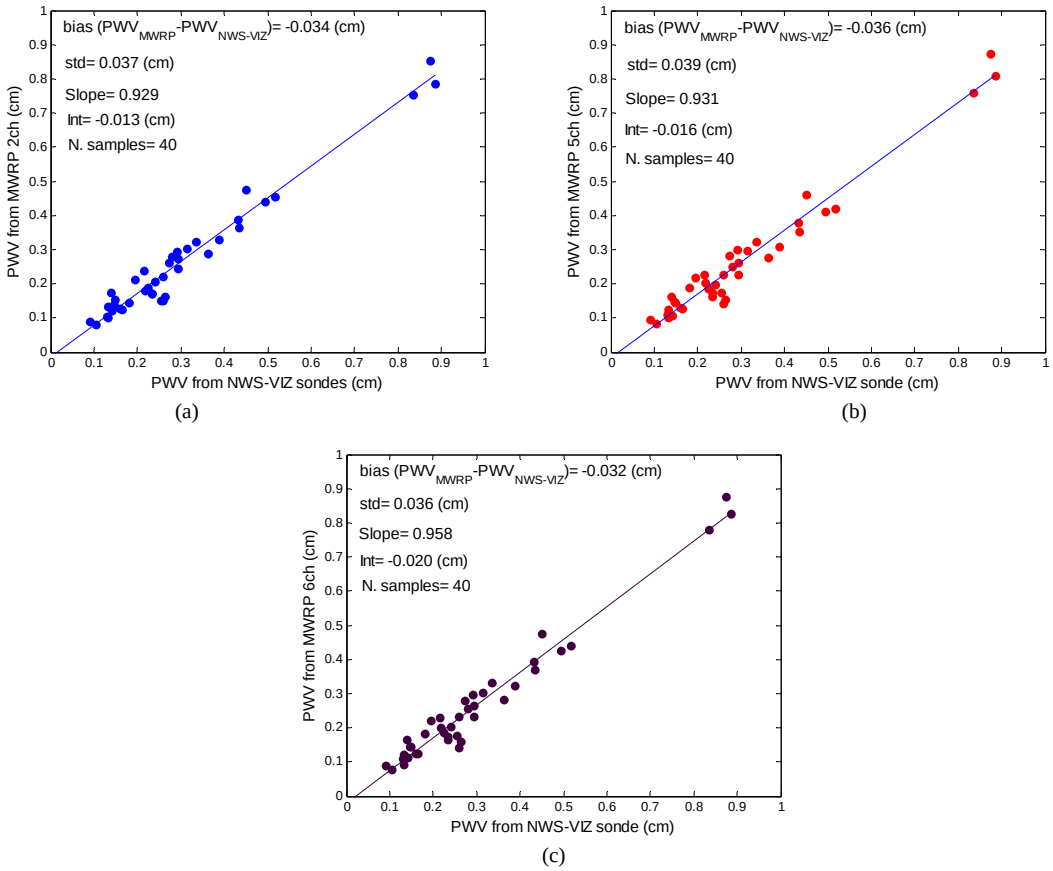

Figure 27. PWV from the MWRP compared with PWV from the NWS-VIZ sondes: (a) comparison for the MWRP 2-channel retrieval, (b) for the 5-channel retrieval, (c) for the 6-channel retrieval.

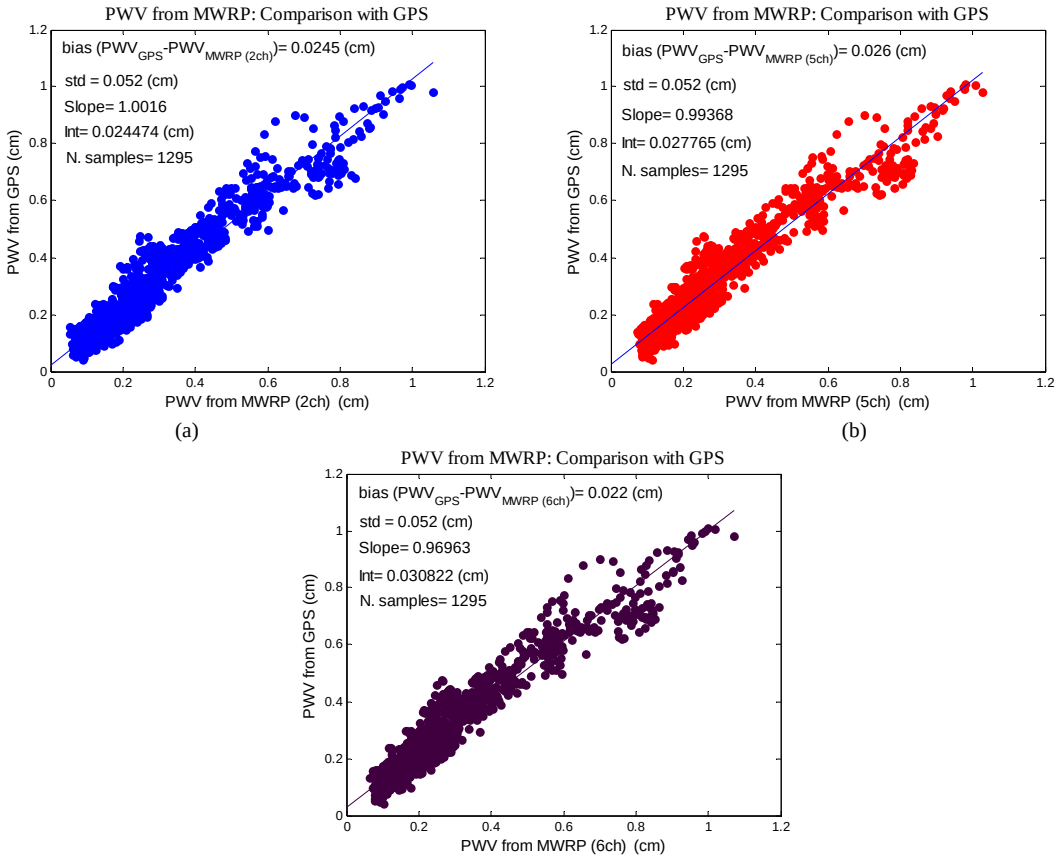

Figure 28. PWV from GPS compared with PWV from the MWRP (a) retrieved by using 2 channels, (b) retrieved by using 5 channels, (c) and by using 6 channels.

Table 3. Rms difference of PWV from RAOBs compared with PWV from the MWR C1, the GPS and the MWRP. Sample size is given in parentheses.

rms (cm)

	DPLX-RS90 sondes	GW-RS90 sondes	NWS-VIZ sondes
MWR (ARM calibration)	0.038 (104)	0.057 (25)	0.041 (42)
MWR (ETL calibration)	0.035 (104)	0.056 (25)	0.035 (42)
GPS	0.069 (112)	0.115 (26)	0.069 (44)
MWRP (2-channel retrieval)	0.023 (100)	0.041 (26)	0.050 (40)
MWRP (5-channel retrieval)	0.028 (100)	0.042 (26)	0.053 (40)
MWRP (6-channel retrieval)	0.029 (100)	0.045 (26)	0.048 (40)